Transcription factor activity and nucleosome organisation in mitosis

Pablo Navarro Gil, Nicola Festuccia, Nick Owens, Thaleia Papadopoulou, Inma González, Alexandra Tachtsidi, Sandrine Vandormael-Pournin, Elena Gallego, Nancy Gutierrez, Agnès Dubois, et al.

Transcription factor activity and nucleosome organisation in mitosis

Nicola Festuccia[1, 4], Nick Owens[1, 4], Thaleia Papadopoulou[1], Inma Gonzalez[1], Alexandra Tachtsidi[1, 3], Sandrine Vandoermel-Pournin[2], Elena Gallego[1], Nancy Gutierrez[1], Agnès Dubois[1], Michel Cohen-Tannoudji[2], and Pablo Navarro[1, 5]

1: Epigenetics of Stem Cells, Department of Developmental and Stem Cell Biology, Institut Pasteur, CNRS UMR3738, 25 rue du Docteur Roux, 75015 Paris, France. Equipe Labellisée LIGUE Contre le Cancer.

2: Mouse Functional Genetics, Department of Developmental and Stem Cell Biology, Institut Pasteur, CNRS UMR 3738, 25 rue du Docteur Roux, 75015 Paris, France.

3: Sorbonne Université, Collège Doctoral, F-75005 Paris, France.

4: equal contribution

5: correspondence should be sent to P.N. pnavarro@pasteur.fr

Abstract

Mitotic bookmarking transcription factors (BFs) maintain the capacity to bind to their targets during mitosis, despite major rearrangements of the chromatin. While they were thought to propagate gene regulatory information through mitosis by statically occupying their DNA targets, it has recently become clear that BFs are highly dynamic in mitotic cells. This represents both a technical and a conceptual challenge to study and understand the function of BFs: first, formaldehyde has been suggested to be unable to efficiently capture these transient interactions, leading to profound contradictions in the literature; second, if BFs are not permanently bound to their targets during mitosis, it becomes unclear how they convey regulatory information to daughter cells. Here, comparing formaldehyde to alternative fixatives we clarify the nature of the chromosomal association of previously proposed BFs in embryonic stem cells: while ESRRB can be considered as a canonical BF that binds at selected regulatory regions in mitosis, SOX2 and POU5F1 (also known as OCT4) establish DNA sequence independent interactions with the mitotic chromosomes, either throughout the chromosomal arms (SOX2) or at pericentromeric regions (POU5F1). Moreover, we show that ordered nucleosomal arrays are retained during mitosis at ESRRB bookmarked sites, whereas regions losing transcription factor binding display a profound loss of order. By maintaining nucleosome positioning during mitosis, ESRRB might ensure the rapid post-mitotic re-establishment of functional regulatory complexes at selected enhancers and promoters. Our results provide a mechanistic framework that reconciles dynamic mitotic binding with the transmission of gene regulatory information across cell division.

248 words

Introduction

During mitosis, the chromatin is drastically condensed and reconfigured to enable the equitable partition of the genetic material between the two daughter cells (Ma et al. 2015). This leads to a strong decrease in transcriptional activity and to the general reduction of transcription factor (TF) binding throughout the genome. Loss of TF binding is further accentuated by the stereotypical phosphorylation of many regulators during mitosis, leading to an intrinsic reduction of their ability to bind DNA. This is particularly well illustrated by the systematic phosphorylation of C2H2 zinc finger TFs such as YY1 (Rizkallah et al. 2011; Rizkallah and Hurt 2009), but has also been observed for other TFs such as POU5F1 (also known as OCT4) and SOX2 (Shin et al. 2016; Qi et al. 2016). Moreover, the breakdown of the nuclear envelope, and the consequent increase of the volume that TFs can freely explore, leads to a decrease of TF concentration. This process naturally inhibits the ability of TFs to scan DNA for their binding motifs. Therefore, many processes occur simultaneously to temporarily halt gene regulation and transcription during mitosis.

The mechanisms by which daughter cells accurately re-establish an environment permissive for efficient transcriptional activation early in interphase remain unknown (de Castro et al. 2016). One potential mechanism is known as mitotic bookmarking: some TFs have the ability to interact with their DNA binding sites during cell division. These TFs, known as mitotic bookmarking factors (BFs), are believed to directly convey gene regulatory information from mother to daughter cells, as illustrated by GATA1 (Kadauke et al. 2012), FOXA1 (Caravaca et al. 2013) and ESRRB (Festuccia et al. 2016). Nonetheless, the molecular mechanisms underpinning this function remain to be elucidated (Festuccia et al. 2017). BFs are highly dynamic during mitosis and often exhibit reduced residence times on the chromatin. Therefore, the function of BFs is not simply mediated by their stable retention at enhancers and promoters. Instead, their transient binding activity may preserve specific chromatin features at bookmarked sites. These features would represent the inherited properties driving and accelerating the reassembly of functional regulatory complexes early in the following interphase. Remarkably, even though the chromatin is highly condensed during mitosis, gene regulatory elements remain globally accessible (Hsiung et al. 2015). This is particularly true at active promoters, perhaps reflecting their low but nevertheless significant mitotic activity, as recently reported (Palozola et al. 2017). Enhancers, in contrast, show more variable degrees

of chromatin accessibility. Yet, mitotic chromatin accessibility does not seem to correlate with mitotic binding, at least in the case of bookmarking by GATA1 in erythroblasts (Kadauke et al. 2012). Moreover, the maintenance of chromatin accessibility does not preclude the possibility that nucleosome positioning in mitotic cells is highly modified, as previously suggested (Kelly et al. 2010; Javasky et al. 2018). Hence, further studies are required to clarify whether regulatory elements do indeed maintain a local chromatin architecture compatible with TF binding in mitotic cells, and how mitotic bookmarking correlates with and ultimately drives nucleosome organisation.

An essential condition to understand mitotic bookmarking processes is to accurately identify BFs and their mitotic binding sites. However, this has remained a difficult task because, as reported nearly 15 years ago (Pallier et al. 2003), the most commonly used cross-linker, formaldehyde, leads to the artificial depletion of TFs from mitotic chromosomes (Pallier et al. 2003; Teves et al. 2016). To circumvent this problem mitotic bookmarking activity has been explored using live imaging of tagged TFs. Even so, whether the global chromatin association of certain TFs detected by microscopy reflects the sum of site-specific interactions remains to be demonstrated. Diverse modes of binding, others than those involving base-specific interactions, may be responsible for the global decoration of the chromosomes by TFs, as we proposed earlier (Festuccia et al. 2017) and was clearly demonstrated for FOXA1 (Caravaca et al. 2013). These interactions with the chromatin, or with other constituents of mitotic chromosomes, might be extremely transient and not easily captured by formaldehyde. In support of this distinction between global and site-specific interactions, several TFs have been efficiently captured at their mitotic binding sites using formaldehyde (Festuccia et al. 2017), despite its seeming incapacity to cross-link TFs on mitotic chromosomes. Yet, it remains to be proven whether formaldehyde generally fails in capturing DNA sequence-specific interactions, leading to the loss of enrichment of BFs on the chromosomes, or whether the interactions sustaining the global retention of BFs are distinct from those involved in TF binding to DNA. This does not only represent an important technical question; rather, it directly interrogates the nature and, hence, the function, of the interactions established between TFs and mitotic chromosomes: while global, dynamic and DNA sequence-independent interactions may increase the concentration of TFs in the vicinity of DNA, possibly facilitating the re-establishment of binding in the following interphase, authentic mitotic bookmarking of promoters and enhancers may confer specificity to these processes and

provide robustness to the post-mitotic resuscitation of gene regulatory networks. In this manuscript, we use mouse Embryonic Stem (ES) cells to study the capacity of different fixatives to crosslink pluripotency TFs either globally on the chromosomes or locally at gene regulatory regions during mitosis. We subsequently use this information to correlate TF binding with chromatin accessibility and nucleosome positioning and stability in interphase and mitosis.

Results

The global localisation of ESRRB to mitotic chromosomes is preserved upon DSG fixation.

Several TFs have been shown to seemingly coat the mitotic chromosomes when fusion proteins with fluorescent proteins or tags are used in live imaging approaches (Festuccia et al. 2017). This is the case of ESRRB (Festuccia et al. 2016), which we previously showed decorates mitotic chromatin using GFP (Fig. 1A), Tdtomato and Snap-tag fusions in mouse ES cells. However, upon formaldehyde fixation, several TFs capable of coating the mitotic chromosomes, seem to be globally delocalised and crosslinked outside of the chromosomes (Pallier et al. 2003; Teves et al. 2016). We first aimed to test whether this is also the case for ESRRB. As expected, we observed a clear depletion from the mitotic chromosomes (Fig. 1B), which were identified by DAPI (Supplemental Fig. S1) and Ki-67 staining (Fig. 1B), a protein enriched on their periphery (Booth and Earnshaw 2017). We therefore aimed at identifying alternative cross-linking agents that would preserve the chromosomal enrichment of ESRRB. Among the different reagents and protocols that we tested (Supplemental Methods), we found two that clearly allow to visualise ESRRB coating of the mitotic chromosomes. First, the homobifunctional crosslinker disuccinimidyl glutarate (DSG), which combined to formaldehyde (DSG+FA; Fig. 1B and Supplemental Fig. 1) has been used to capture hyper-dynamic protein-protein interactions due to its capacity to establish amide bonds via two NHS-ester groups (Tian et al. 2012). Second, Glyoxal (Supplemental Fig. S1), a small bifunctional aldehyde that has been recently rediscovered for its use in fluorescent microscopy (Richter et al. 2018). With both fixatives, ESRRB is detected covering the entire area delimited by Ki-67, within the chromatin compartment (Fig. 1B and Supplemental Fig. S1). As a control, we stained ES cells for NANOG (Fig. 1A), a TF that is excluded from the mitotic chromatin (Festuccia et al. 2016). Upon DSG+FA or Glyoxal fixation, we did not observe retention of NANOG on mitotic chromosomes (Fig. 1B and Supplemental Fig. S1), indicating that these two cross-linkers do

not induce aspecific aggregation on the chromosomes. We also tested whether DSG would allow us to visualise the global chromosomal retention of ESRRB *in vivo*. We have shown before that upon microinjection of *Esrrb-Tdtomato* mRNA into mouse embryos, the produced fluorescent fusion proteins decorate the mitotic chromatin (Festuccia et al. 2016). Accordingly, when we fixed mouse blastocysts with DSG+FA we could observe mitotic figures with a clear coating of the chromosomes by ESRRB but not by NANOG (Fig. 1C).

DSG fixation does not alter the profile of ESRRB binding in mitotic cells.

Our finding that DSG and Glyoxal maintain the global association of ESRRB with the mitotic chromosomes opens the possibility to test whether this binding results from the sum of site-specific interactions or from other mechanisms. Indeed, if the global staining reflected site-specific interactions exclusively, one should expect to identify a much larger number of ESRRB binding sites by Chromatin Immuno-Precipitation (ChIP) after fixation with DSG or Glyoxal than with FA. Yet, despite our efforts, we could not perform ChIP with these two reagents; in contrast, after a double crosslinking with DSG followed by FA (DSG+FA), which is frequently used in biochemical approaches (Tian et al. 2012), ChIP was particularly efficient. Therefore, we performed ChIP-seq in asynchronous (hereafter interphase) and mitotic preparations of ES cells (>95% purity); after splitting the populations in two, we proceeded in parallel with either FA or DSG+FA crosslinking. We observed very similar profiles of ESRRB binding both in interphase and in mitosis, irrespective of whether the cells had been crosslinked with FA or with DSG+FA (Fig. 1D and Supplemental Fig. S2). Therefore, whereas ESRRB is globally cross-linked outside or within the mitotic chromosomes by FA and DSG respectively, the mitotic ChIP signal does not vary dramatically. We note however that DSG+FA provides higher ChIP signal and better signal to background ratio, both in interphase and in mitosis. In agreement with immunostaining and live imaging, NANOG binding is globally lost, both in FA and in DSG+FA (Fig. 1D and Supplemental Fig. S2). From this analysis, we conclude that the global coating and the interaction of ESRRB with specific sites are two distinct phenomena. While mitotic ESRRB bookmarking (i.e. binding to specific sites) can be revealed by FA and by DSG+FA, the global coating visible by microscopy is only preserved by DSG (or Glyoxal).

DSG versus FA comparisons reveal different behaviours of other proposed BFs.

In addition to ESRRB, other pluripotency TFs have been proposed to act as BFs in ES cells (Deluz et al. 2016; Teves et al. 2016; Liu et al. 2017), although evidence is contradictory. SOX2 has been consistently shown by microscopy to globally associate with mitotic chromosomes in three independent studies (Deluz et al. 2016; Teves et al. 2016; Liu et al. 2017). In contrast, while one study (Deluz et al. 2016) reported by ChIP-seq that SOX2 binds with poor efficiency to a few dozen regions in mitosis (compared to thousands of sites in interphase), another study claimed that SOX2 and POU5F1 remain bound to virtually all their interphase targets (Liu et al. 2017). In addition, SOX2 and POU5F1 were shown to be phosphorylated by Aurora kinases, which inhibit DNA binding in mitotic cells (Qi et al. 2016; Shin et al. 2016). These studies performed ChIP after FA fixation, which leads to an apparent depletion from mitotic chromosomes of both SOX2 and POU5F1 (Fig. 2A, C). In contrast, we found that SOX2 displays bright signal all over the chromosomal arms, within the Ki-67 delimited region, by immunostaining after DSG+FA and Glyoxal fixation (Fig. 2A and Supplemental Fig. S1). We thus extended our ChIP-seq analysis based on DSG+FA fixation to SOX2. Whereas DSG+FA dramatically increases ChIP efficiency of SOX2 compared to FA, the profiles in mitosis are very similar for both fixatives, with little evidence for mitotic bookmarking activity (Fig. 2C and Supplemental Fig. S2). Therefore, while displaying a global behaviour similar to ESRRB, mitotic SOX2 does not appear to be an efficient BF. Next, we analysed POU5F1 binding. By immunofluorescence, we observed a nearly complete depletion from the chromosomal arms in mitosis, both after DSG+FA and Glyoxal (Fig. 2C and Supplemental Fig. S1). In agreement, ChIP-seq analysis also showed almost complete loss of POU5F1 binding at its interphase targets (Fig. 2D and Supplemental Fig. S2). Our results are in agreement with a number of other studies (Deluz et al. 2016; Shin et al. 2016; Kim et al. 2018). However, even using DSG+FA we could not reproduce recent results showing mitotic bookmarking by SOX2 and POU5F1 (Liu et al. 2017). The use of inhibitors of MEK/GSK3b in the conflicting publication, which leads to a reinforcement of the pluripotency network's activity, cannot account for these differences (Supplemental Fig. S3). Considering that only site-specific interactions mediate mitotic bookmarking activity (Festuccia et al. 2017), and that only residual signal can be detected at some POU5F1/SOX2 regions (Fig. 2B and Supplemental Fig. S2), we conclude from our data that neither SOX2 nor POU5F1 can be considered as potent BFs. Hence, while a global enrichment of TFs can be detected on the chromatin by microscopy, the establishment of site-

specific interactions with regulatory elements is a property of selected bookmarking factors like ESRRB.

DSG enables capturing transient interactions at different chromatin compartments.

The global retention of SOX2 on mitotic chromosomes was validated using live imaging of ectopically expressed SOX2-GFP (Fig. 3A top). Similarly, the large exclusion of POU5F1 was also confirmed by live imaging (Fig. 3A bottom). Careful examination of the POU5F1 stainings (after DSG+FA and Glyoxal, but not FA fixation; Fig. 2C and Supplemental Fig. S1), as well as of unfixed POU5F1-GFP (Fig. 3A bottom), did however unmask a previously unnoticed accumulation of this TF at DAPI-rich regions, the chromocenters (Saksouk et al. 2015), where several centromeres cluster together to form peri-centric heterochromatin (PCH); white arrowheads in Fig. 2C). Moreover, in mitotic cells we could also observe focal enrichment of POU5F1 at centromeric regions (filled-white arrowheads in Fig. 2C and in Supplemental Fig. S1). This characteristic pattern of co-localisation with the PCH was further validated by live imaging using endogenously expressed POU5F1-RFP fusion proteins (Supplemental Fig. S4A). Same results were obtained in cells cultured in regular conditions or with inhibitors of MEK/GSK3b (Supplemental Fig. S4A). In the latter conditions, PCH shifts from H3K9me3 to H3K27me3 (Tosolini et al. 2018), indicating that the PCH association of POU5F1 is independent of the presence of specific heterochromatic marks. Notably, Aurora kinase b, which has been shown to phosphorylate POU5F1 in mitotic cells to inhibit DNA binding (Qi et al. 2016; Shin et al. 2016), also stains PCH in interphase and the centromeres in mitosis (Supplemental Fig. S4B). Moreover, in the presence of the Aurora kinase inhibitor Hesperadin a slight increase of POU5F1 coating throughout the chromosomal arms could be observed (Supplemental Fig. S4C). Hence, using alternative fixatives to FA not only enables the visualisation of the genuine mitotic localisation of TFs, but may also reveal additional activities in interphase. We then asked whether the interactions of SOX2 and POU5F1 unmasked by DSG and Glyoxal are indeed dynamic, as generally reported (Teves et al. 2016). We observed highly dynamic interactions, both in interphase and in mitosis, for all three factors fused to GFP and analysed in parallel experiments (Fig. 3B, C, and Supplemental Fig. S5). ESRRB and POU5F1 displayed faster fluorescent recovery after photobleaching (FRAP) in mitosis than in interphase (Fig. 3B, C). This is particularly true for the interaction of POU5F1 with PCH, which is already very dynamic in interphase (Fig. 3C). In reciprocal experiments, we assessed fluorescence loss in

photobleaching (FLIP; Supplemental Fig. S5). We could not identify any significant remnant signal on mitotic chromatids after one minute of continuous bleaching of the freely diffusing TF molecules. Hence, DSG (and Glyoxal) are capable of capturing the highly dynamic interactions established by ESRRB/SOX2 on the chromosomal arms, and by POU5F1 in PCH.

ESRRB is the only prominent BF among ESRRB, SOX2, POU5F1 and NANOG.

Using the collection of datasets generated for ESRRB, SOX2, POU5F1 and NANOG in interphase and in mitosis (Supplemental Table S1 provides an overview of the samples and their relevant statistics), we sought to comprehensively identify regions subject to mitotic bookmarking. To this end, we first identified the binding regions of individual TFs (listed in Supplemental Table S2; Supplemental Fig. S6) and confirmed that only ESRRB displays clear and frequent binding in mitosis (Fig. 4A); for POU5F1, SOX2 and NANOG, only the regions displaying very high levels of binding in interphase show residual ChIP signal in mitosis, especially in DSG+FA, where the number of detected peaks is increased in both conditions. Peaks that were called only in DSG+FA, and neither in our FA samples nor in other publicly available datasets (Chen et al. 2008; Marson et al. 2008; Aksoy et al. 2013; Whyte et al. 2013), tend to be smaller (Supplemental Fig. S7). Nevertheless, their signal is clearly above background in all the analysed datasets of interphase cells fixed with FA (Supplemental Fig. S7). Hence, DSG helps capturing regions displaying low levels of binding and increases the overall efficiency of the ChIP. Nonetheless, it does not specifically unmask new binding in mitosis. We then used a statistical differential occupancy approach to define regions as bookmarked or lost (see Supplemental Methods for details and Supplemental Table S2). We found 10,144 regions bookmarked by ESRRB, representing 29.9% of its interphase sites. All other factors displayed a drastic contraction in binding in mitosis: 574 regions for SOX2 (2% of interphase targets); 102 regions for POU5F1 (0.6%); 18 regions for NANOG (0.07%). Strong ESRRB binding motifs were identified at the vast majority of ESRRB bookmarked regions (Fig. 4B left; 73.4%, score > 12), but only at a smaller subset of the regions losing binding in mitosis (34.9%, score > 12). In contrast, regions losing ESRRB binding displayed an increased occurrence of POU5F1/SOX2 composite motifs (Fisher $p<7\times10^{-45}$, score > 12). We observed a scaling relationship: regions containing high quality POU5F1/SOX2 motifs, exhibit a higher tendency to lose ESRRB binding in mitosis (Fig. 4B right). Previously, we used titration experiments to investigate whether the binding levels seen for ESRRB in mitosis could be explained by contamination from interphase

(Festuccia et al. 2016); all our mitotic preparations have less than 5% of remnant interphase cells, and typically between 2 and 4%. We repeated this analysis for SOX2, given the relatively high number of low mitotic peaks that we detected in comparison to POU5F1 and NANOG. To produce SOX2-depleted chromatin, we generated an ES cell line with (i) both endogenous *Sox2* alleles tagged with an auxin-inducible degradation domain (producing SOX2-AID fusion), and (ii) a constitutive transgene expressing the TIR1 protein inserted at the *Tigre* locus (Madisen et al. 2015). Upon treatment with the auxin analogue IAA for 2h, a significant reduction of SOX2-AID levels was observed (Fig. 4C). To further deplete SOX2, cells were differentiated in the presence of retinoic acid (RA) and IAA for 4 days. Gradually increasing amounts of WT chromatin were then spiked into chromatin prepared from IAA-RA treated cells, and ChIP-seq analysis performed. We found that as little of 5% of WT chromatin was sufficient to detect clear SOX2 peaks of reduced enrichment (Fig. 4D). The amount of signal observed by adding 5% of contaminant chromatin was higher, on average, to that seen in mitosis at the regions potentially bookmarked by SOX2 (Fig. 4D). Therefore, it is possible that a significant fraction of the regions seemingly bound by SOX2 in mitosis, as well as the absolute levels of enrichment in mitosis, results from the small percentage of contaminant interphase cells in our preparations. To further corroborate that SOX2 is not an efficient bookmarking factor we turned to a functional assay. Confirming our previous results, the set of ESRRB bookmarked regions identified here tend to be enriched in the vicinity of genes that are controlled by this TF in early G1 (Fig. 4E; Festuccia et al. 2016). We then introduced a GFP-CCNA cell-cycle reporter (Festuccia et al. 2016) into SOX2-AID cells, treated them with IAA for 2h and sorted early G1 cells to perform RNA-seq analyses. In comparison with ESRRB, we found a rather minor statistical association between the genes controlled by SOX2 in early G1 (Supplemental Table S3) and the regions potentially bookmarked by SOX2 (Fig. 4E). We conclude that, whilst we cannot fully rule out that SOX2 may display minimal bookmarking activity, only ESRRB represents a potent and functionally relevant BF among the tested pluripotency factors. This conclusion is particularly well illustrated when the ChIP signal measured at each region is plotted in interphase versus mitosis (Fig. 4A; bottom panels), or when the proportion of reads on peaks are calculated for each TF (Fig. 4F). Why SOX2 and POU5F1 have been previously found mitotically bound at most of their interphase targets (Liu et al. 2017) remains therefore unclear. This is particularly striking, taking into consideration that our DSG+FA datasets clearly display improved ChIP efficiency compared to several other published profiles (Fig. 4F).

Despite our efforts, and the addition of 3 and 2 additional independent replicates for SOX2 and POU5F1, respectively (red dots in Fig. 4F), we did not find strong evidence for SOX2 and POU5F1 bookmarking.

Drastic changes in nucleosome organisation characterise regulatory elements in mitosis.

Recently, mitotic chromatin has been shown to maintain high levels of chromatin accessibility at virtually all regulatory elements that are active in interphase, in particular at promoters (Hsiung et al. 2015; Teves et al. 2016). Accordingly, we observed that promoter accessibility in mitotic ES cells even surpasses the level observed in interphase, as evaluated by ATAC-seq (Fig. 5A and Supplemental Figure S8A). However, distinct nucleosome organisations might characterise accessible chromatin in these two phases of the cell cycle (Kelly et al. 2010; Teif et al. 2014; Rhee et al. 2014; Mieczkowski et al. 2016; Voong et al. 2016; Mueller et al. 2017; Javasky et al. 2018). To address this, we inferred nucleosome positioning and stability in interphase and in mitosis from a series of experiments based on MNase-seq and H3 ChIP-seq using chromatin digested with titrated MNase activity. We first analysed promoter regions and observed preserved nucleosome depleted regions (NDR) around the transcription start sites in mitotic cells (TSS; Fig. 5B). Yet, the phasing of nucleosomes at both sides of the NDRs was drastically attenuated in mitotic cells (Fig. 5B), probably reflecting reduced transcriptional activity. Moreover, when we compared average H3 ChIP-seq signal between mitosis and interphase at different levels of MNase digestion (Fig. 5C and Supplemental Fig. S8B), a clear asymmetry was revealed: upstream of the TSS, the sensitivity of the nucleosomes to MNase increased in mitotic cells (as shown by reduced signal with strong digestion); downstream, the +1 nucleosome displayed a similar stability than in interphase, while the following nucleosomes acquired in mitosis increasing levels of fragility. At the minimal promoter region (TSS and 150bp upstream), we did not find evidence of a nucleosome displaying high occupancy either in interphase or in mitosis (Fig. 5B and Supplemental Fig. S8B). Nonetheless, the H3 signal detected over the minimal promoter tends to increase in mitosis, irrespectively of the MNase conditions (Fig. 5C and Supplemental Fig. S8B). These results indicate that, globally, the nucleosomes at promoters are more fragile (Teif et al. 2014; Mieczkowski et al. 2016; Voong et al. 2016) in mitosis, except at the minimal promoter region where they display unaltered stability and similar occupancy. Moreover, the differential behaviour within and outside the transcription unit may potentially reflect the reduced transcriptional activity that

has been recently detected in mitotic cells (Palozola et al. 2017). Therefore, promoters are subject to drastic nucleosome reorganisation in mitotic cells. We then analysed enhancers (identified here as EP300-bound elements, excluding TSSs and gene bodies). As previously shown (Hsiung et al. 2015), we found enhancers to partially lose accessibility in mitosis (Fig. 5D and Supplemental Fig. 8A) and display a profound reconfiguration in nucleosomal architecture (Fig. 5E) that is particularly well revealed with increasing MNase activity (Supplemental Fig. S8B): nucleosomes resistant to our most aggressive digestion conditions can be detected at the site of EP300 recruitment exclusively in mitosis, and the phasing of the surrounding nucleosomes is altered (Fig. 5E and Supplemental Fig. S8B). Moreover, both upstream and downstream of the stabilised nucleosome, increased fragility can be measured in mitotic cells (Fig. 5F and Supplemental Fig. S8B). Therefore, even though promoters and enhancers maintain significant levels of accessibility in mitotic cells, the arrangement of their nucleosomes changes substantially.

Chromatin accessibility and nucleosome organisation as a function of ESRRB bookmarking.

We then focused on the analysis of the regions bound by ESRRB. While ESRRB-bookmarked regions partially lose accessibility (Fig. 6A), this reduction is significantly more pronounced at the regions where ESRRB binding is lost in mitosis (Fig. 6C). Hence, there is a clear correlation between the ability of ESRRB to bind to certain targets in mitotic cells, and the partial maintenance of accessibility. Moreover, at bookmarked regions, we observed highly positioned nucleosomes both in interphase and mitosis: the ESRRB motif lies within a major NDR and phased nucleosomes spread both upstream and downstream the binding site (Fig. 6B and Supplemental Fig. S9A). This pattern contrasts markedly with that seen at EP300 enhancers (Fig. 5E), clearly establishing a strong correlation between ESRRB mitotic binding and the retention of well-structured nucleosome arrays. Moreover, in mitosis we observed a slight shrinking of the nucleosomal array converging towards the central ESRRB motif, leading to a modest change of position of the nucleosomes. Remarkably, when we calculated a frequency map of additional ESRRB motifs within these regions (grey histogram in Fig. 6B), we observed a small but clear enrichment precisely at the mitosis-specific inter-nucleosomal space between the -2/-1 and +1/+2 nucleosomes. This strongly indicates that in mitosis, the DNA binding activity of ESRRB becomes dominant in establishing nucleosome positioning. In contrast, at regions losing ESRRB binding in mitosis, the nucleosomes appeared barely

organised compared to their bookmarked counterparts: a nucleosome occupies the ESRRB motif, particularly in mitosis, and clear phasing is lacking at both sides (Fig. 6D). Since high quality ESRRB motifs are not particularly prevalent at these regions (Fig. 4B), we reanalysed the data by re-centring on ESRRB summits. We noted that POU5F1/SOX2 motifs are enriched in the vicinity of ESRRB summits (grey histogram in Fig. 6E), and therefore also re-centred these regions on these motifs (Fig. 6F and Supplemental Fig. S9A). Both analyses unveiled a clear nucleosomal organisation in interphase that is highly modified in mitotic cells (Fig. 6E, F). This indicates that ESRRB may be recruited indirectly and play a minor role in establishing nucleosome positioning over these regions. In accord, the nucleosome pattern at regions centred on ESRRB summits was also highly similar to that seen at the bulk of POU5F1/SOX2 binding sites (Fig. 6H and Supplemental Fig. S10A). These regions show a consistent reduction in accessibility in mitosis (Fig. 6G) and major nucleosome repositioning, with signs of shifting in the nucleosomal array and invasion at both flanks of the POU5F1/SOX2 motifs (Fig. 6H). At all these regions, a concomitant increase in occupancy by fragile nucleosomes could also be observed (Supplemental Figs. S9 and S10). Of note, the presence of a more stable nucleosome at specific positions, like the ones we observed at TSSs and EP300 summits, could not be detected at ESRRB or POU5F1/SOX2 binding sites in mitotic cells (Fig. 5E, F and Supplemental Fig. S9B and S10B). Finally, at regions exhibiting low mitotic SOX2 ChIP-seq signal, we also observed major reorganisations of nucleosomes in mitosis. Nonetheless, the presence of a very narrow NDR in mitosis could not be ruled out (Supplemental Fig. S11), possibly reflecting minimal bookmarking activity. From these analyses, we conclude that TF binding is likely required to maintain nucleosome positioning at regulatory elements during cell division. ESRRB acts as a major organiser of the chromatin in both phases of the cell cycle (Fig. 6B).

Discussion

Proposed around 20 years ago (Michelotti et al. 1997), the idea that certain TFs mitotically propagate gene regulatory information had been until recently only sporadically explored. Instead, over the last few years, several publications have revealed a continuously growing number of candidate mitotic bookmarking TFs (Festuccia et al. 2017). Considering that FA, arguably the most used cross-linker, leads to an artificial depletion of TFs from the mitotic chromosomes, as visualised by microscopy (Pallier et al. 2003; Teves et al. 2016), many more TFs than those currently described are probably able to associate with the chromatin during division, as recently suggested (Cai et al. 2018; Raccaud et al. 2018; Ginno et al. 2018). However, whether all these TFs are engaged in site-specific interactions and therefore act as mitotic bookmarking factors remains unclear (Festuccia et al. 2017). Here, we identify cross-linkers that preserve the global mitotic localisation detected by microscopy for several TFs, providing a simple experimental method to study the behaviour of new transcriptional regulators during division and, more generally, visualise spatial organisations deriving from transient and fast binding events. Conversely, our results impose caution: we show that localisation of a TF to the chromatin does not necessarily imply DNA sequence-specific binding in mitosis (Fig. 7A). This is exemplified by SOX2 and, as shown by others, by CTCF (Oomen et al. 2018): while these TFs are both chromosomally retained, they are largely evicted from the sites occupied in interphase. The functional consequences of this distinction are major: we failed to identify a strong relationship between the weak and sparse binding of SOX2 in mitotic ES cells and its transcriptional effects in early G1. Conversely, the functional relevance of site-specific mitotic binding (Fig. 7) has been documented for several canonical bookmarking factors, including GATA1 (Kadauke et al. 2012), FOXA1 (Caravaca et al. 2013) and ESRRB (Festuccia et al. 2016). Therefore, the emerging idea of a widespread mitotic bookmarking activity needs to be carefully considered and evaluated. At the same time, the potential function of a global chromosomal retention cannot be ignored and requires dedicated experimental setups. In this regard, our comparative analysis of fixatives reveals that distinct molecular mechanisms likely contribute to the overall mitotic localisation of TFs (Fig. 7B). ESRRB displays highly correlated binding profiles by ChIP when the chromatin is fixed with FA or with DSG+FA. In contrast, only DSG captures global ESRRB enrichment on the chromatin. Given the ability of DSG to efficiently fix transient interactions, and in light of the results of

FRAP and single molecule tracking studies (Caravaca et al. 2013; Deluz et al. 2016; Teves et al. 2016; Raccaud et al. 2018), this reveals that most likely the bulk of the molecules for a given TF bound to the chromatids during mitosis are not engaged in sequence-specific interactions with DNA. However, we showed previously that mutating 3 amino-acids of the ESRRB DNA biding domain that are engaged in base-specific contacts with the binding motif, dramatically decreases the global decoration of the mitotic chromosomes (Festuccia et al. 2016). It is possible that these amino acids of the ESRRB zinc-finger domain are also required for ESRRB to scan the DNA in search of its biding sites. Alternatively, these mutations may more generally alter the structure of ESRRB, preventing interactions with other proteins enriched on mitotic chromosomes. Notably, the bifunctional cross-linkers that we have used, DSG and Glyoxal, are expected to increase the efficiency of fixation within large protein complexes, opening the possibility that the interactions driving the global enrichment of TFs on the chromatids are based on protein-protein rather than protein-DNA contacts. Thus, we suggest that the model previously proposed for FOXA1 regarding the existence of at least two distinct phenomena underlying the behaviour of TFs in mitotic cells could be extended, and applied generally to BFs: on the one hand, both DNA scanning and the ability to interact with other proteins of the chromatin sustains the bulk localisation of TFs to the chromatids; on the other, bona-fide bookmarking, understood here as the capacity to mediate site-specific binding, drives functionally relevant accumulation of TFs at regulatory elements (Festuccia et al. 2017). While FOXA1 is capable of binding nucleosomes directly (Cirillo et al. 1998), by virtue of its inherent structural properties (Clark et al. 1993; Ramakrishnan et al. 1993), the mitotic partners involved in protein-protein interactions with other TFs decorating mitotic chromosomes may be more diverse (Fig. 7B). These proteins could be part of the chromatin or restricted to the chromosomal periphery (Booth and Earnshaw 2017). While our co-staining with Ki-67 excludes the possibility of such restricted localisation for ESRRB, SOX2 and POU5F1, this may apply to other TFs. Indeed, a multitude of determinants of TF localisation seem to exist. This is the case of POU5F1, that we report here as focally enriched within (peri-)centric regions, both in interphase and in mitosis. Extending beyond mitosis, given the complexity revealed by the use of multiple cross-linking agents, this study directly calls for a general reassessment of TF localisation and function as inferred from fixed samples.

Distinguishing TFs as enriched or depleted from mitotic chromosomes, and as binding or not at specific regulatory regions, will eventually allow us to establish a hierarchy of their contributions to the re-establishment of transcription after mitosis (Fig. 7). This will be particularly important in highly proliferative cells undergoing progressive implementation of new cell identities during development (Festuccia et al. 2017). To gain a full understanding of the importance of mitotic bookmarking, it is also crucial to elucidate the molecular mechanisms mediating its function. Different lines of evidence point to the lack of permanent TF binding during mitosis; even in the extreme case of the general TF TBP, the residence time on the mitotic chromatin is below 2 minutes (Teves et al. 2018). Therefore, static occupancy by single molecules of mitotic bookmarking factors do not physically transfer regulatory information from mother to daughter cells; to be functional, BFs may instead induce specific modifications around their mitotic target sites. However, regardless of their mitotic bookmarking status, most if not all active regulatory regions remain at least partially accessible in mitotic cells (Hsiung et al. 2015; Teves et al. 2016). This has been now shown analysing the binding sites of several TFs, including GATA1 (Kadauke et al. 2012), and, here, ESRRB, SOX2 and POU5F1 (Fig. 7A). Therefore, even if many other BFs remain to be identified, the general loss of TF binding characterising mitosis is unlikely to completely abolish chromatin accessibility. In general, the presence of destabilised nucleosomes at regulatory elements could suffice to maintain these regions less refractory to the binding of transcriptional regulators. Nevertheless, TF binding might still contribute towards maintaining comparatively high accessibility at selected loci. This was originally proposed for the bookmarking factor FOXL1 (Yan et al. 2006) and is further supported by our observation that the regions bookmarked by ESRRB display a milder reduction of ATAC signal compared to those where ESRRB is evicted. More significantly, our nucleosome mapping studies indicate that ESRRB bookmarking plays a major role in preserving the fine patterns of nucleosome organisation, rather than mere accessibility, at regulatory elements (Fig. 7). Indeed, at regions bookmarked by ESRRB, binding motifs are strongly associated with a nucleosome depleted region, and are flanked by well organised and phased nucleosomes. This configuration is detected in interphase, but is significantly clearer in mitosis where even neighbouring inter-nucleosomal spaces correlate with the presence of additional ESRRB motifs. We believe this reflects the loss of counteracting effects from binding of other TFs in mitosis, and the consequent dominance of ESRRB over the organisation of the nucleosomes at these sites. In

this light, mitosis might represent a context of simplified interactions of TFs with the chromatin, where few fundamental activities are maintained. In contrast, in the complete absence of mitotic TF binding, nucleosomal arrays are largely reconfigured. This is true at enhancers marked by EP300, at regions losing ESRRB and/or POU5F1/SOX2 binding, as well as at CTCF binding sites (Oomen et al. 2018). Remarkably, at regions losing ESRRB in mitosis a clear nucleosomal organisation is only appreciated when regions are aligned relative to the ESRRB peak summit or the binding motifs for POU5F1/SOX2. Hence, at these regions, ESRRB might be recruited indirectly by other TFs that are not capable of binding in mitosis, such as POU5F1/SOX2: the nucleosomal organisation of these regions, therefore, is not likely to be imposed by ESRRB. Together these observations clearly indicate that mitotic bookmarking by ESRRB is essentially driven by sequence-specific DNA interactions through which this factor imposes specific constraints on nucleosomal organisation. In this light, the nucleosomal landscape around TF binding sites in mitosis may be used as a proxy for mitotic bookmarking activity, further indicating that neither SOX2 nor POU5F1 are efficient bookmarking factors.

The recent observation of widespread chromatin accessibility in mitotic cells suggested that many TFs would act as bookmarking factors, a notion that is further supported by recent results derived from large imaging and proteomic screens (Cai et al. 2018; Raccaud et al. 2018; Ginno et al. 2018). In contrast, our analysis of TF binding, chromatin accessibility, nucleosome positioning and stability in mitotic cells, rather indicates that mitotic bookmarking can only be mediated by selected TFs, such as ESRRB in ES cells. Indeed, the stereotypical behaviour of enhancers that we observe here indicates that a robust nucleosome is positioned at EP300 recruitment sites, with more fragile nucleosomes occupying the vicinities. These destabilised nucleosomes may explain the apparent accessibility of these regions. At promoters, we also observe a loss of phasing, and a relative stabilisation of the nucleosomes lying just upstream of the TSS as compared to those more distally located, which appear to be more fragile. While the identification of the molecular players destabilising these nucleosomes will require further investigation, our data indicate that ESRRB, and potentially other bookmarking factors, may generally act by locally preserving specific nucleosome architectures. These configurations might in turn favour the re-establishment of functional regulatory complexes early after mitosis. We propose this mechanism to represent the molecular basis of the transmission of regulatory information by sequence-specific mitotic bookmarking factors (Fig. 7B).

Methods

Cell culture, embryos and fixation. Mouse ES cells (E14Tg2a) were grown on FCS and LIF, unless indicated, on gelatine coated flasks. For imaging, they were plated on IBIDI plates coated with poly-L-ornithine and laminin. Blastocysts were collected at E3.25 and cultured for five hours in KSOM. GFP fusion proteins were ectopically expressed using CAG-driven vectors. *Sox2*-AID ES cells were generated in ES cells expressing a *Ccna*-GFP reporter to perform cell-cycle sorting as previously described (Festuccia et al. 2016). Fixation of ES cells was performed with either formaldehyde (FA; 1% for ChIP and 4% for stainings during 10 min), disuccinimidyl glutarate (DSG; 2mM for 50 min) followed by FA, or glyoxal (3.1% for 30 min); embryos were fixed for 24h in DSG followed by 20' in FA. The detailed protocols are available on the Supplemental Methods.

Chromatin preparation in mitotic ES cells. E14Tg2a cells were grown to 70-80% confluency, incubated with nocodazole (50ng×ml^{-1} for 4 to 5h) and mitotic cells shake-off as detailed in Supplemental Methods, reaching a purity above 95%. After fixation, chromatin was prepared as previously described (Festuccia et al. 2016) and either sonicated with a Bioruptor Pico (Diagenode) for TF binding analysis by ChIP-seq, digested with different amounts of MNase (0.5/16/128U) for MNase-seq and H3 ChIP-seq, or processed for ATAC-seq analysis as previously described (Buenrostro et al. 2013). Detailed protocols and experimental procedures can be found on the Supplemental Methods.

Sequencing and bioinformatics analyses. TF ChIP-seq libraries were sequenced (SR50-75) at the BioMics facility of the Institut Pasteur; all other libraries were sequenced (PE150) by Novogene Co. Ltd. At least two biological replicates were sequenced per experiment. Reads were aligned with Bowtie 2 (Langmead and Salzberg 2012) to the mm9 genome. ChIP-seq peaks were identified by MACS2 (Feng et al. 2012) and analysed by a Generalised Linear Model with DESeq2 (Love et al. 2014) to identify genomic sites of mitotic bookmarking; TF binding motifs were identified with FIMO (Grant, Bailey, and Noble 2011). Chromatin accessibility was analysed counting the cut-sites of 0-100bp paired-end fragments obtained by ATAC-seq across regions of interest, and smoothed with a Gaussian Process Regression. Nucleosome positioning was inferred from MNase-seq and MNase-H3 ChIP-seq, taking into

consideration the mid-points of 140-200bp paired-end fragments. Mid-points counts were corrected to the natural bias of MNase, assessed in each library by a *k*-mer approach. Subsequently, we used Gaussian process regression to evaluate nucleosome positioning signals. All the procedures and normalisations are described in detail in the Supplemental Methods.

Data access

All genome wide datasets have been deposited to the NCBI Gene Expression Omnibus (GEO; https://www.ncbi.nlm.nih.gov/geo), under the accession number GSE122589.

Acknowledgments

The authors acknowledge the Imagopole France–BioImaging infrastructure, supported by the French National Research Agency (ANR 10-INSB-04-01, Investments for the Future), for advice and access to the UltraVIEW VOX system. We also acknowledge the Transcriptome and EpiGenome, BioMics, Center for Innovation and Technological Research of the Institut Pasteur for NGS. We are grateful to Elphège Nora and Benoit Bruneau for sharing reagents and advice to establish the auxin-dependent degradation system. This work was supported by recurrent funding from the Institut Pasteur, the CNRS, and Revive (Investissement d'Avenir; ANR-10-LABX-73). P.N. acknowledges financial support from the Fondation Schlumberger (FRM FSER 2017), the Agence Nationale de la Recherche (ANR 16 CE12 0004 01 MITMAT), and the Ligue contre le Cancer (LNCC EL2018 NAVARRO). N.F was supported by a Marie Curie IEF fellowship and a Pasteur-Cantarini Fellowship program. N.O. is supported by Revive.

Author contributions:

N.F. performed or supervised most of the experimental work. N.O. analysed sequencing data. T.P. performed ChIP-seq, ATAC-seq, confocal microscopy and Western Blots. I.G. setup the ATAC protocol and performed ChIP-seq in 2i ES cells. A.T. performed live imaging, confocal microscopy and all experiments relating to POU5F1 localisation, with help from N.G. Embryo work was performed by S.V.P. and M.C.T. The fixation protocols were initially tested by E.G. and A.D. Data analysis and interpretation, as well as writing the manuscript, was performed by N.F., N.O. and P.N.

Disclosure declaration: The authors declare no competing interests.

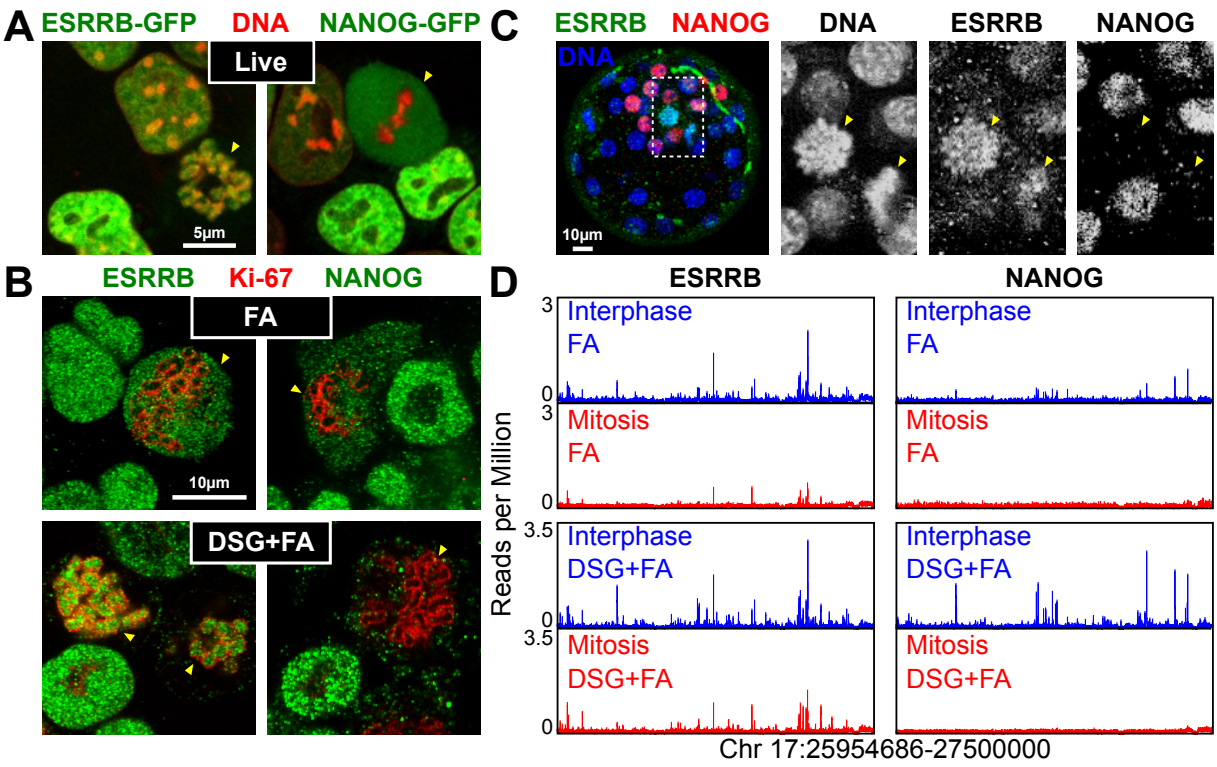

Figure 1: Capturing global ESRRB binding on mitotic chromosomes. (A) Localisation of ESRRB-GFP (left) or NANOG-GFP (right) fusion proteins in live cells cultured with Hoechst 33342 (red). **(B)** ESRRB (left) and NANOG (right) immunofluorescence (green) after fixation with either FA (top) or DSG+FA (bottom). The chromosome periphery of mitotic chromosomes is identified by Ki-67 (red). **(C)** Immunostaining for NANOG (red) or ESRRB (green) performed on a mouse blastocyst fixed with DSG+FA. Counterstain with Hoechst 33342 is shown in blue. Close-up on two mitotic cells is shown in the right panels (dashed area delimits the selected region). Mitotic cells are indicated in (A-C) with yellow arrowheads. **(D)** Representative binding profiles of ESRRB and NANOG across 1.5Mb in interphase (blue) or mitosis (red), obtained after fixation with either FA (top) or DSG+FA (bottom).

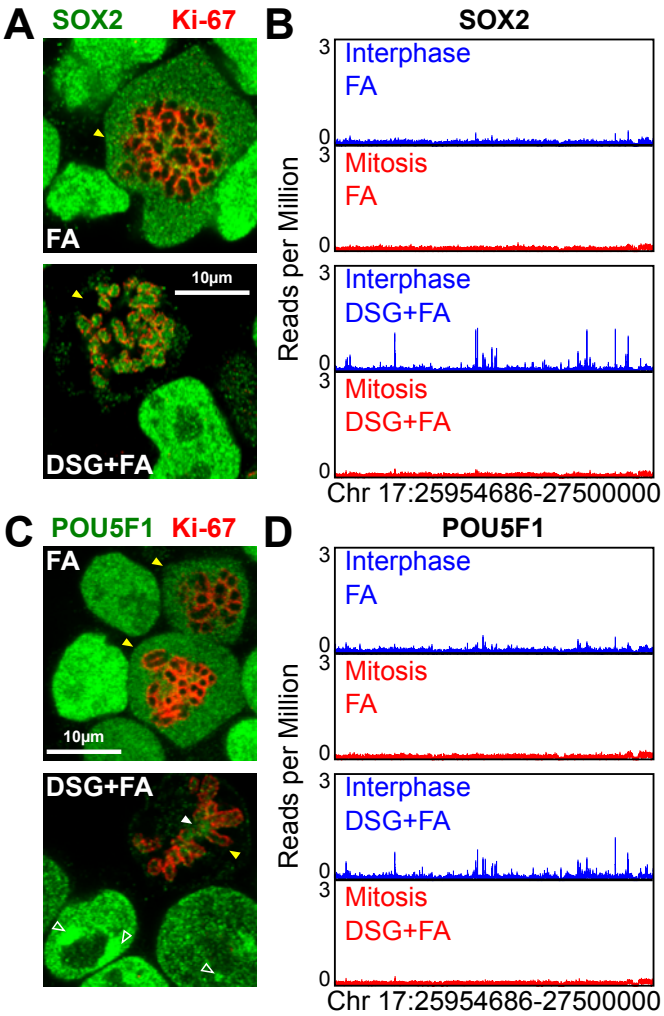

Figure 2: SOX2 and POU5F1 do not bind at regulatory regions in mitosis. (A) SOX2 immunofluorescence (green), after fixation with either FA (top) or DSG+FA (bottom). The mitotic chromosome periphery is identified by Ki-67 (red). **(B)** Representative binding profiles of SOX2 presented as in Fig. 1D. **(C, D)** Results of the same analyses described in (A) and (B) are shown for POU5F1. Mitotic cells are indicated in (A, C) with yellow arrowheads. In (C), the filled white arrowheads point to the centromeres; the empty white arrowheads to the PCH.

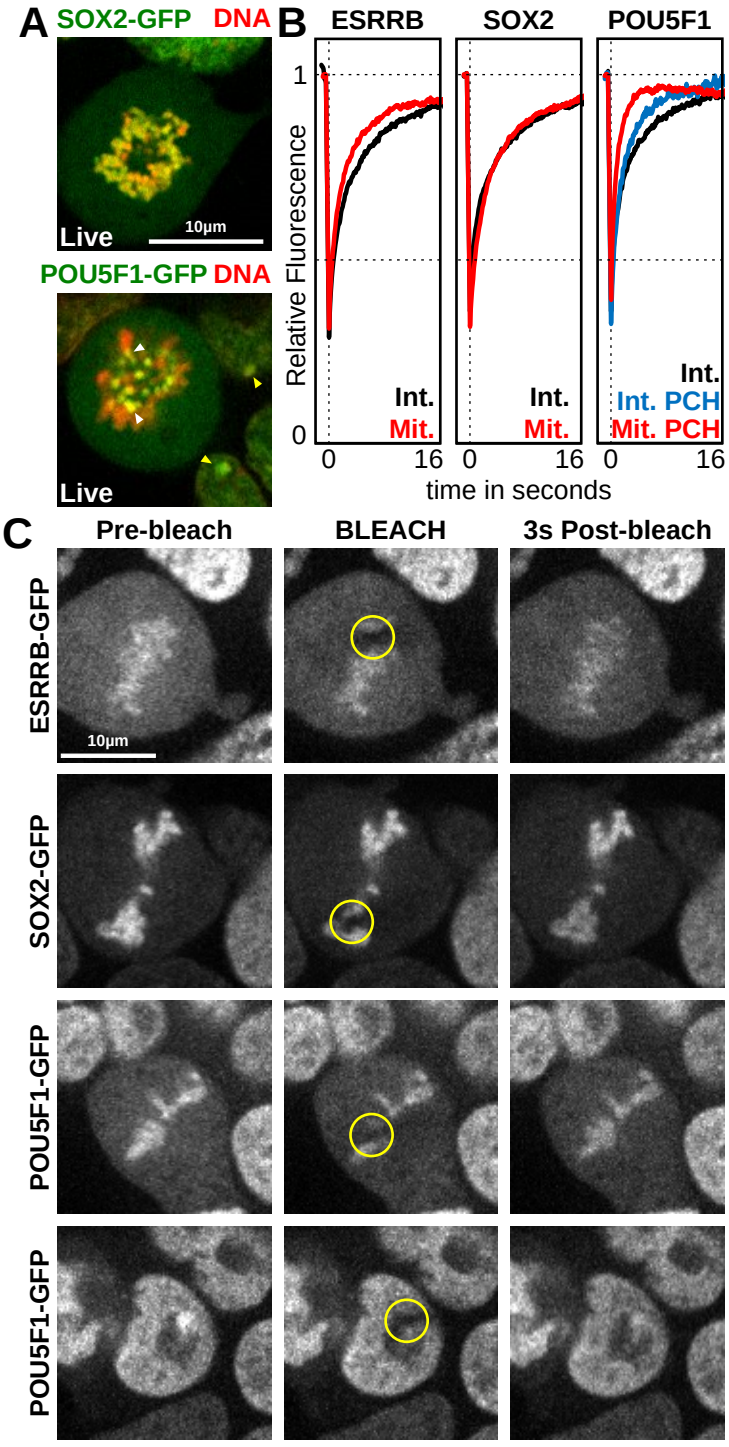

Figure 3: The interactions captured by DSG are dynamic. (A) Localisation of SOX2-GFP (top) or POU5F1-GFP (bottom) fusion proteins (green) in live cells cultured with Hoechst 33342 (red). Arrowheads indicate peri-centric heterochromatin foci (PCH) in interphase (yellow) and centromeres in mitosis (white). **(B)** Quantifications of FRAP experiments in interphase (black) and mitosis (red) performed in cells expressing ESRRB-GFP or SOX2-GFP. For cells expressing POU5F1-GFP, recovery of fluorescence at (blue), or outside of (black), peri-centric heterochromatin foci (PCH) is displayed for interphase. Recovery at PCH is displayed for mitosis (red). The Y axis shows the mean percentage of fluorescence relative to pre-bleach levels detected in multiple independent experiments; the X axis shows the time after bleaching. **(C)** Representative examples of ESRRB-GFP, SOX2-GFP and POU5F1-GFP signal on mitotic chromosomes before and after bleaching, at the indicated time. For POU5F1-GFP the recovery of signal at PCH is also shown for cells in interphase (bottom).

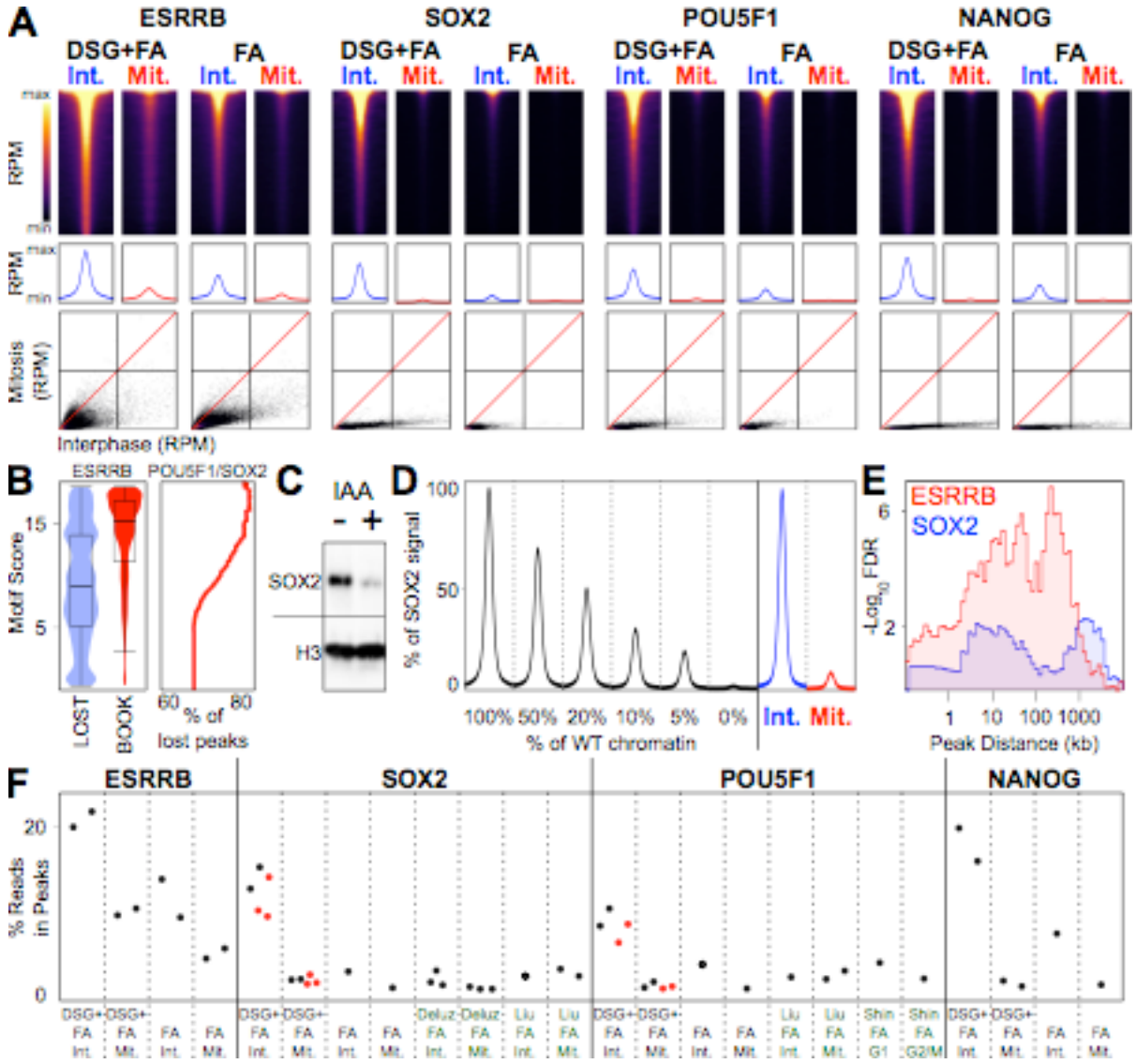

Figure 4: Comparative analysis of ESRRB, SOX2, POU5F1 and NANOG binding in interphase and in mitosis. (A) Top: heatmaps of ChIP-seq signal at the indicated binding regions (+/- 500bp peak summit) identified in interphase (Int.) and mitosis (Mit.) for DSG+FA and FA alone. Middle: average binding profile of the regions shown in the heatmaps. Heatmaps and average binding profiles display Reads per Million (RPM), the Y axis differs for each factor and is scaled by median DSG+FA Interphase binding: ESRRB: 0-1.5 RPM, SOX2: 0-3.2 RPM, POU5F1: 0-2.6 RPM; NANOG: 0-2.7 RPM. Bottom: scatter plots of ChIP-seq signal in Reads per Million (RPM) at the above regions for interphase and mitosis (DSG+FA scale 0-40 RPM; FA scale 0-20 RPM). **(B)** Violin plots (left) depicting the FIMO-called best motif score per ESRRB peak in sites losing binding in mitosis (LOST) or retaining binding (BOOK). Right: percentage of Lost peaks with a composite POU5F1/SOX2 motif of at least the given quality score. **(C)** Levels of SOX2-AID fusion protein in cells cultured in the absence (-) or presence (+) of the Auxin analogue IAA for

2 hours; H3 is shown as control. **(D)** Percent of the SOX2 ChIP signal detected at binding regions after spiking increasing amounts of WT chromatin into chromatin prepared from SOX2-depleted cells shown alongside the average SOX2 binding profile at potentially bookmarked regions in WT cells in interphase and mitosis. **(E)** Enrichment of genes responsive to ESRRB (red) and SOX2 (blue) in early G1 as a function of the distance to ESRRB or SOX2 bookmarked regions, respectively, displayed as $-\log_{10}$ Fisher FDR. **(F)** Percentage of ChIP-seq reads in identified binding sites for ESRRB, SOX2, POU5F1 and NANOG, in both interphase (Int.) and mitosis (Mit.) and DSG+FA or FA fixation in our data (black labels) and public datasets (green labels). The red dots correspond to the samples that were added to our study to further corroborate our results.

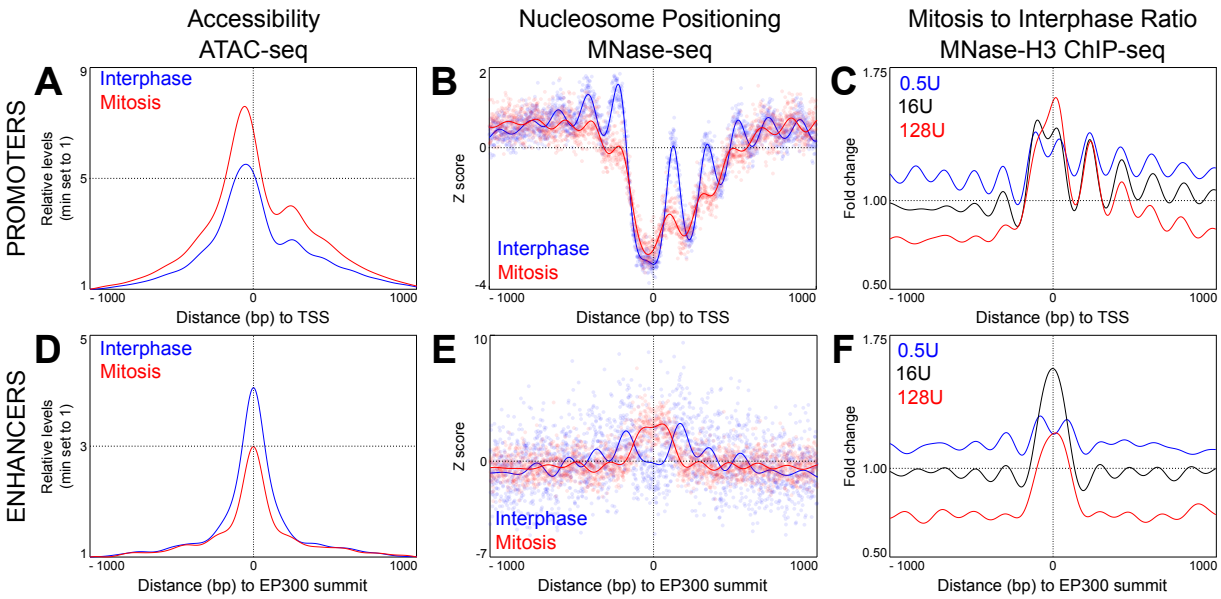

Figure 5: The nucleosome landscape of promoters and enhancers in interphase and in mitosis. (A) Accessibility profiles measured by ATAC-seq in the region surrounding the TSS of active genes in interphase (blue) or mitosis (red). Signal is number of Tn5 cut sites for 0-100 bp fragments, normalised to minimum accessibility in +/- 1000 bp window. Depth normalised data can be found in Supplemental Fig. S8B. See Supplemental Methods for details. **(B)** Nucleosome positioning at the same set of promoters, established by MNase-seq. In this panel, the z-score of the number of midpoints of nucleosome-sized fragments (140-200bp) per base, after digestion with 16U of enzyme, are plotted. The lines represent a Gaussian process modelling nucleosome positioning (see Supplemental Methods) in interphase (blue) and in mitosis (red). **(C)** Mitosis over interphase ratio of MNase H3 ChIP-seq signal for nucleosomal fragments (as assessed by Gaussian process regression; see Supplemental Methods). Ratios shown for MNase digestions with 0.5U (blue), 16U (black) and 128U (red) of enzyme. Since this analysis aims at identifying quantitative changes in nucleosome occupancy, we used H3 data as not all MNase nucleosome sized fragments are guaranteed to contain a nucleosome. **(D, E, F)** as (A, B, C) but for regions centred on summits of interphase EP300 ChIP-seq peaks excluding promoters. Note that in (E) MNase-seq signal is from 128U digestions. Full datasets can be found in Supplemental Fig. S8B.

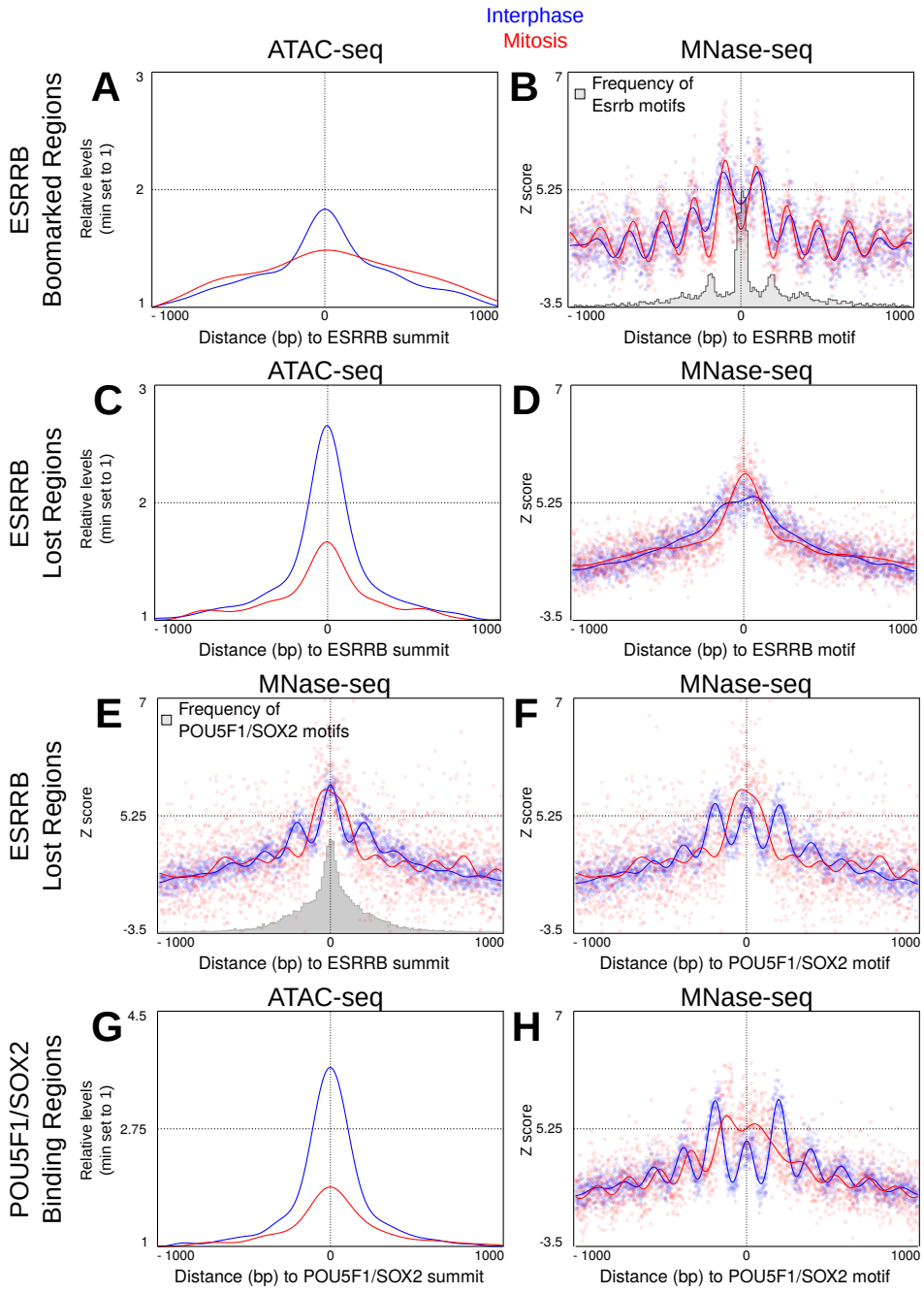

Figure 6: Binding of ESRRB at its cognate motif correlates with nucleosome organisation in interphase and in mitosis. Accessibility **(A, C, G)** determined by ATAC-seq as in Fig. 5A, and nucleosome positioning **(B, D, E, F, H)** established as in Fig. 5B, at the regions indicated on the left and centred as shown on their corresponding X-axis, in interphase (blue) and mitosis (red). Histograms embedded in (B) and (E), depict rate of occurrence of the indicated binding motifs: (B) additional ESRRB motifs with FIMO score > 8; (E) top scoring POU5F1/SOX2 composite motifs.

A

	Global Mitotic Behavior			Mitotic Site-Specific binding	Chromatin Status	
	Live	FA	DSG/Glyoxal	FA or DSG+FA	Accessibility	Nucleosomes
ESRRB	coating	exclusion	coating	BOOKMARKING	retained	ordered
				eviction	reduced	disorganised
NANOG	exclusion	exclusion	exclusion	eviction	n.a	n.a
SOX2	coating	exclusion	coating	eviction	reduced	disorganised
POU5F1	centromeric	exclusion	centromeric	eviction	reduced	disorganised

B

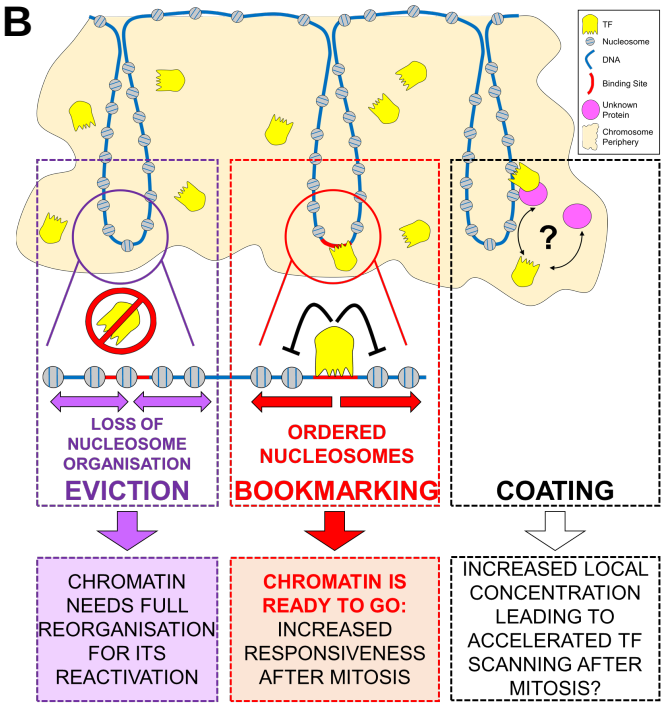

Figure 7: Model summarising distinct behaviours of pluripotency TFs in mitotic cells and their relationships to nucleosome organisation and post-mitotic gene regulation. (A) Summary table of the behaviour of ESRRB, NANOG, SOX2 and POU5F1 in mitotic mouse ES cells. **(B)** Many TFs show global localisation on the chromosomes in mitosis, such as ESRRB and SOX2. This localisation is likely driven by sequence-independent interactions with DNA or other components of the chromatin or of the mitotic chromosomes, and might serve a function in increasing the local concentration of TFs in proximity of their targets, in turn facilitating binding in G1. In contrast, during division only few TFs remain dynamically bound to a subset of the sites they occupy in interphase, as exemplified by ESRRB. At bookmarked sites, the continued activity of these TFs maintains an ordered chromatin configuration, possibly limiting the extent of chromatin remodelling required to re-establish functional regulatory architectures in the following cell-cycle. At sites losing TF binding, nucleosome positioning is disorganised, and increased occupancy by nucleosomes is detected at binding motifs. Although these sites do not become fully inaccessible, profound chromatin rearrangements are expected to be needed in early G1 to reinstate proper function.

References

Aksoy I, Jauch R, Chen J, Dyla M, Divakar U, Bogu GK, Teo R, Leng Ng CK, Herath W, Lili S et al. 2013. Oct4 switches partnering from Sox2 to Sox17 to reinterpret the enhancer code and specify endoderm. *EMBO J* **32**: 938-953.

Booth DG, Earnshaw WC. 2017. Ki-67 and the Chromosome Periphery Compartment in Mitosis. *Trends Cell Biol* **27**: 906-916.

Buenrostro JD, Giresi PG, Zaba LC, Chang HY, Greenleaf WJ. 2013. Transposition of native chromatin for fast and sensitive epigenomic profiling of open chromatin, DNA-binding proteins and nucleosome position. Nat Methods 10(12): 1213-1218.

Cai Y, Hossain MJ, Hériché JK, Politi AZ, Walther N, Koch B, Wachsmuth M, Nijmeijer B, Kueblbeck M, Martinic-Kavur M, Ladurner R, et al. 2018. Experimental and computational framework for a dynamic protein atlas of human cell division. *Nature*. **561**: 411-415.

Caravaca JM, Donahue G, Becker JS, He X, Vinson C, Zaret KS. 2013. Bookmarking by specific and nonspecific binding of FoxA1 pioneer factor to mitotic chromosomes. *Genes Dev* **27**: 251-260.

Chen X, Xu H, Yuan P, Fang F, Huss M, Vega VB, Wong E, Orlov YL, Zhang W, Jiang J et al. 2008. Integration of external signaling pathways with the core transcriptional network in embryonic stem cells. *Cell* **133**: 1106-1117.

Cirillo LA, McPherson CE, Bossard P, Stevens K, Cherian S, Shim EY, Clark KL, Burley SK, Zaret KS. 1998. Binding of the winged-helix transcription factor HNF3 to a linker histone site on the nucleosome. *EMBO J* **17**: 244-254.

Clark KL, Halay ED, Lai E, Burley SK. 1993. Co-crystal structure of the HNF-3/fork head DNA-recognition motif resembles histone H5. *Nature* **364**: 412-420.

de Castro IJ, Gokhan E, Vagnarelli P. 2016. Resetting a functional G1 nucleus after mitosis. *Chromosoma* **125**: 607-619.

Deluz C, Friman ET, Strebinger D, Benke A, Raccaud M, Callegari A, Leleu M, Manley S, Suter DM. 2016. A role for mitotic bookmarking of SOX2 in pluripotency and differentiation. *Genes Dev* **30**: 2538-2550.

Feng J, Liu T, Qin B, Zhang Y, Liu XS. 2012. Identifying ChIP-seq enrichment using MACS. Nat Protoc 7(9): 1728-1740.

Festuccia N, Dubois A, Vandormael-Pournin S, Gallego Tejeda E, Mouren A, Bessonnard S, Mueller F, Proux C, Cohen-Tannoudji M, Navarro P. 2016. Mitotic binding of Esrrb marks key regulatory regions of the pluripotency network. *Nat Cell Biol* **18**: 1139-1148.

Festuccia N, Gonzalez I, Owens N, Navarro P. 2017. Mitotic bookmarking in development and stem cells. *Development* **144**: 3633-3645.

Ginno PA, Burger L, Seebacher J, Iesmantavicius V, Schübeler D. 2018. Cell cycle-resolved chromatin proteomics reveals the extent of mitotic preservation of the genomic regulatory landscape. *Nat Commun* **9**: 4048.

Grant, Charles E., Timothy L. Bailey, and William Stafford Noble. 2011. "FIMO: Scanning for Occurrences of a given Motif." Bioinformatics 27 (7): 1017–18.

Hsiung CC, Morrissey CS, Udugama M, Frank CL, Keller CA, Baek S, Giardine B, Crawford GE, Sung MH, Hardison RC et al. 2015. Genome accessibility is widely preserved and locally modulated during mitosis. *Genome Res* **25**: 213-225.

Javasky E, Shamir I, Gandhi S, Egri S, Sandler O, Rothbart SB, Kaplan N, Jaffe JD, Goren A, Simon I. 2018. Study of mitotic chromatin supports a model of bookmarking by histone modifications and reveals nucleosome deposition patterns. *Genome Res*. **28**: 1455-1466.

Kadauke S, Udugama MI, Pawlicki JM, Achtman JC, Jain DP, Cheng Y, Hardison RC, Blobel GA. 2012. Tissue-specific mitotic bookmarking by hematopoietic transcription factor GATA1. *Cell* **150**: 725-737.

Kelly TK, Miranda TB, Liang G, Berman BP, Lin JC, Tanay A, Jones PA. 2010. H2A.Z maintenance during mitosis reveals nucleosome shifting on mitotically silenced genes. *Mol Cell* **39**: 901-911.

Kim HJ, Shin J, Lee S, Kim TW, Jang H, Suh MY, Kim JH, Hwang IY, Hwang DS, Cho EJ et al. 2018. Cyclin-dependent kinase 1 activity coordinates the chromatin associated state of Oct4 during cell cycle in embryonic stem cells. *Nucleic Acids Res* **46**: 6544-6560.

Langmead B, Salzberg SL. 2012. Fast gapped-read alignment with Bowtie 2. Nat Methods 9(4): 357-359.

Liu Y, Pelham-Webb B, Di Giammartino DC, Li J, Kim D, Kita K, Saiz N, Garg V, Doane A, Giannakakou P et al. 2017. Widespread Mitotic Bookmarking by Histone Marks and Transcription Factors in Pluripotent Stem Cells. *Cell Rep* **19**: 1283-1293.

Love MI, Huber W, Anders S. 2014. Moderated estimation of fold change and dispersion for RNA-seq data with DESeq2. Genome Biol 15(12): 550.

Ma Y, Kanakousaki K, Buttitta L. 2015. How the cell cycle impacts chromatin architecture and influences cell fate. *Front Genet* **6**: 19.

Madisen L, Garner AR, Shimaoka D, Chuong AS, Klapoetke NC, Li L, van der Bourg A, Niino Y, Egolf L, Monetti C et al. 2015. Transgenic mice for intersectional targeting of neural sensors and effectors with high specificity and performance. *Neuron* **85**: 942-958.

Marson A, Levine SS, Cole MF, Frampton GM, Brambrink T, Johnstone S, Guenther MG, Johnston WK, Wernig M, Newman J et al. 2008. Connecting microRNA genes to the core transcriptional regulatory circuitry of embryonic stem cells. *Cell* **134**: 521-533.

Michelotti EF, Sanford S, Levens D. 1997. Marking of active genes on mitotic chromosomes. *Nature* **388**: 895-899.

Mieczkowski J, Cook A, Bowman SK, Mueller B, Alver BH, Kundu S, Deaton AM, Urban JA, Larschan E, Park PJ et al. 2016. MNase titration reveals differences between nucleosome occupancy and chromatin accessibility. *Nat Commun* **7**: 11485.

Mueller B, Mieczkowski J, Kundu S, Wang P, Sadreyev R, Tolstorukov MY, Kingston RE. 2017. Widespread changes in nucleosome accessibility without changes in nucleosome occupancy during a rapid transcriptional induction. *Genes Dev* doi:10.1101/gad.293118.116.

Oomen ME, Hansen A, Liu Y, Darzacq X, Dekker J. 2018. CTCF sites display cell cycle dependent dynamics in factor binding and nucleosome positioning. *bioRxiv* doi:10.1101/365866.

Pallier C, Scaffidi P, Chopineau-Proust S, Agresti A, Nordmann P, Bianchi ME, Marechal V. 2003. Association of chromatin proteins high mobility group box (HMGB) 1 and HMGB2 with mitotic chromosomes. *Mol Biol Cell* **14**: 3414-3426.

Palozola KC, Donahue G, Liu H, Grant GR, Becker JS, Cote A, Yu H, Raj A, Zaret KS. 2017. Mitotic transcription and waves of gene reactivation during mitotic exit. *Science* **358**: 119-122.

Qi D, Wang Q, Yu M, Lan R, Li S, Lu F. 2016. Mitotic phosphorylation of SOX2 mediated by Aurora kinase A is critical for the stem-cell like cell maintenance in PA-1 cells. *Cell Cycle* **15**: 2009-2018.

Raccaud M, Alber AB, Friman ET, Agarwal H, Deluz C, Kuhn T, Gebhardt JCM, Suter DM. 2018. Mitotic chromosome binding predicts transcription factor properties in interphase. *bioRxiv* doi:10.1101/404723

Ramakrishnan V, Finch JT, Graziano V, Lee PL, Sweet RM. 1993. Crystal structure of globular domain of histone H5 and its implications for nucleosome binding. *Nature* **362**: 219-223.

Rhee HS, Bataille AR, Zhang L, Pugh BF. 2014. Subnucleosomal structures and nucleosome asymmetry across a genome. *Cell* **159**: 1377-1388.

Richter KN, Revelo NH, Seitz KJ, Helm MS, Sarkar D, Saleeb RS, D'Este E, Eberle J, Wagner E, Vogl C et al. 2018. Glyoxal as an alternative fixative to formaldehyde in immunostaining and super-resolution microscopy. *EMBO J* **37**: 139-159.

Rizkallah R, Alexander KE, Hurt MM. 2011. Global mitotic phosphorylation of C2H2 zinc finger protein linker peptides. *Cell Cycle* **10**: 3327-3336.

Rizkallah R, Hurt MM. 2009. Regulation of the transcription factor YY1 in mitosis through phosphorylation of its DNA-binding domain. *Mol Biol Cell* **20**: 4766-4776.

Saksouk N, Simboeck E, Dejardin J. 2015. Constitutive heterochromatin formation and transcription in mammals. *Epigenetics Chromatin* **8**: 3.

Shin J, Kim TW, Kim H, Kim HJ, Suh MY, Lee S, Lee HT, Kwak S, Lee SE, Lee JH et al. 2016. Aurkb/PP1-mediated resetting of Oct4 during the cell cycle determines the identity of embryonic stem cells. *Elife* **5**: e10877.

Teif VB, Beshnova DA, Vainshtein Y, Marth C, Mallm JP, Hofer T, Rippe K. 2014. Nucleosome repositioning links DNA (de)methylation and differential CTCF binding during stem cell development. Genome Res 24: 1285-1295.

Teves SS, An L, Bhargava-Shah A, Xie L, Darzacq X, Tjian R. 2018. A stable mode of bookmarking by TBP recruits RNA polymerase II to mitotic chromosomes. *Elife* **7**.

Teves SS, An L, Hansen AS, Xie L, Darzacq X, Tjian R. 2016. A dynamic mode of mitotic bookmarking by transcription factors. *Elife* **5**.

Tian B, Yang J, Brasier AR. 2012. Two-step cross-linking for analysis of protein-chromatin interactions. *Supplemental Methods Mol Biol* **809**: 105-120.

Tosolini M, Brochard V, Adenot P, Chebrout M, Grillo G, Navia V, Beaujean N, Francastel C, Bonnet-Garnier A, Jouneau A. 2018. Contrasting epigenetic states of heterochromatin in the different types of mouse pluripotent stem cells. *Sci Rep* **8**: 5776.

Voong LN, Xi L, Sebeson AC, Xiong B, Wang JP, Wang X. 2016. Insights into Nucleosome Organization in Mouse Embryonic Stem Cells through Chemical Mapping. *Cell* **167**: 1555-1570 e1515.

Whyte WA, Orlando DA, Hnisz D, Abraham BJ, Lin CY, Kagey MH, Rahl PB, Lee TI, Young RA. 2013. Master transcription factors and mediator establish super-enhancers at key cell identity genes. *Cell* **153**: 307-319.

Yan J, Xu L, Crawford G, Wang Z, Burgess SM. 2006. The forkhead transcription factor FoxI1 remains bound to condensed mitotic chromosomes and stably remodels chromatin structure. *Mol Cell Biol* **26**: 155-168.

Transcription factor activity and nucleosome organisation in mitosis

Festuccia, N., Owens, N., et al.

SUPPLEMENTAL FIGURES

Supplemental Figure S1:
Comparative analyses of different fixations.

Supplemental Figure S2:
Closer visualisation of a 6kb-long genomic region.

Supplemental Figure S3:
POU5F1 and SOX2 binding in 2i-treated ES cells.

Supplemental Figure S4:
Extended analysis of POU5F1 localisation.

Supplemental Figure S5:
Example of FLIP imaging.

Supplemental Figure S6:
Overview of TF binding sites identification.

Supplemental Figure S7:
Analysis of peaks specifically detected in DSG+FA.

Supplemental Figure S8:
Full ATAC-seq, MNase-seq and MNase-H3 ChIP-seq datasets at promoters and enhancers.

Supplemental Figure S9:
Full MNase and MNase-H3 ChIP-seq datasets at ESRRB binding regions.

Supplemental Figure S10:
Full MNase and MNase-H3 ChIP-seq datasets at POU5F1/SOX2 binding regions.

Supplemental Figure S11:
Chromatin analysis of pseudo-bookmarked SOX2 binding regions.

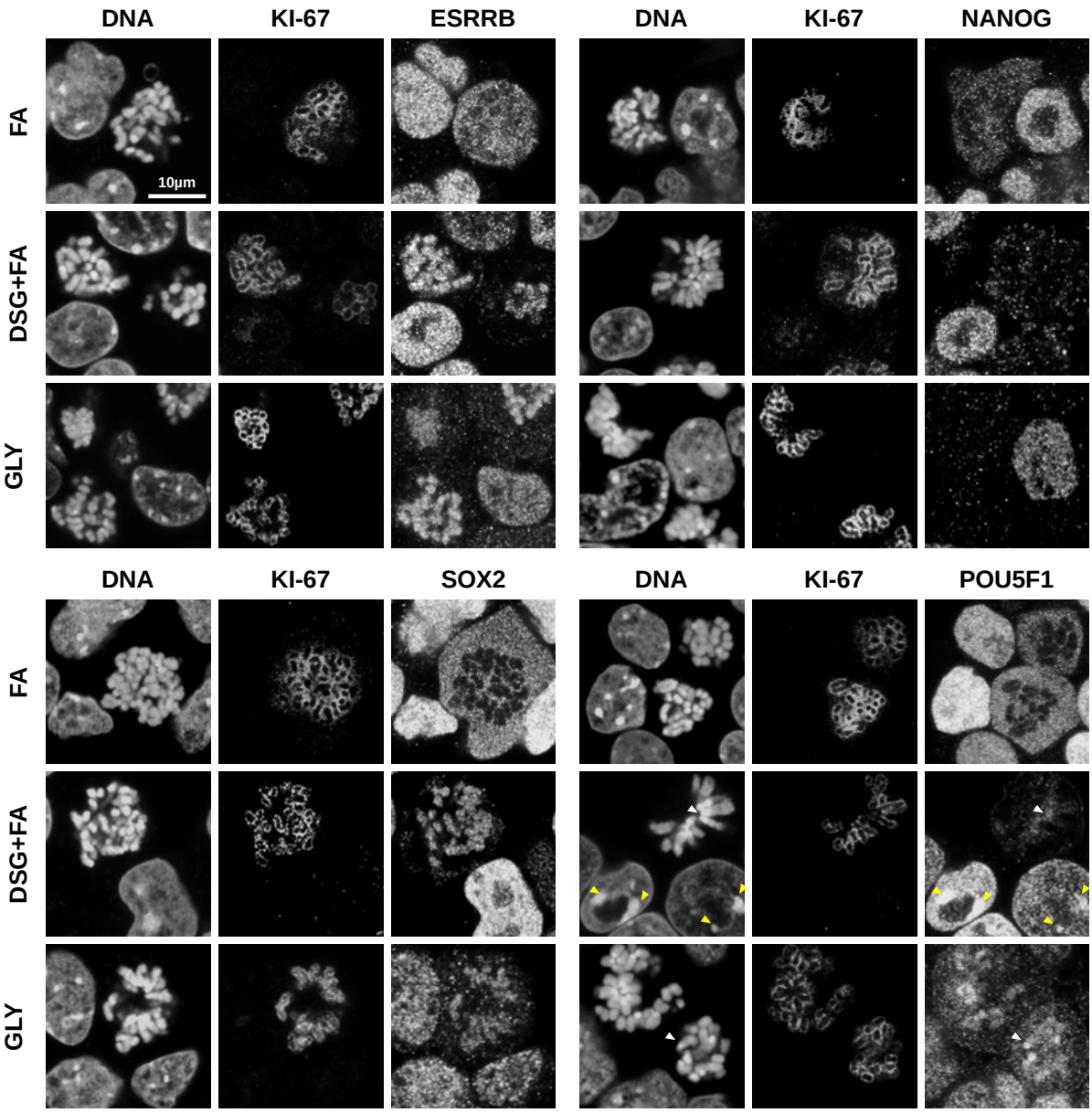

Supplemental Figure S1: Comparative analyses of different fixations. Immunofluorescence for ESRRB (top left), NANOG (top right), SOX2 (bottom left) and POU5F1 (bottom right), after fixation with either FA, DSG+FA, or glyoxal (GLY). DNA was counterstained with DAPI. The mitotic chromosome periphery is identified by KI-67 staining. These images correspond to the single channels of the merged images shown in Figs. 1 and 2. In the POU5F1 staining, the arrowheads indicate peri-centric heterochromatin foci (PCH) in interphase (yellow) and centromeres in mitosis (white). Note that SOX2 immunofluorescence required a FA post-fixation after Glyoxal.

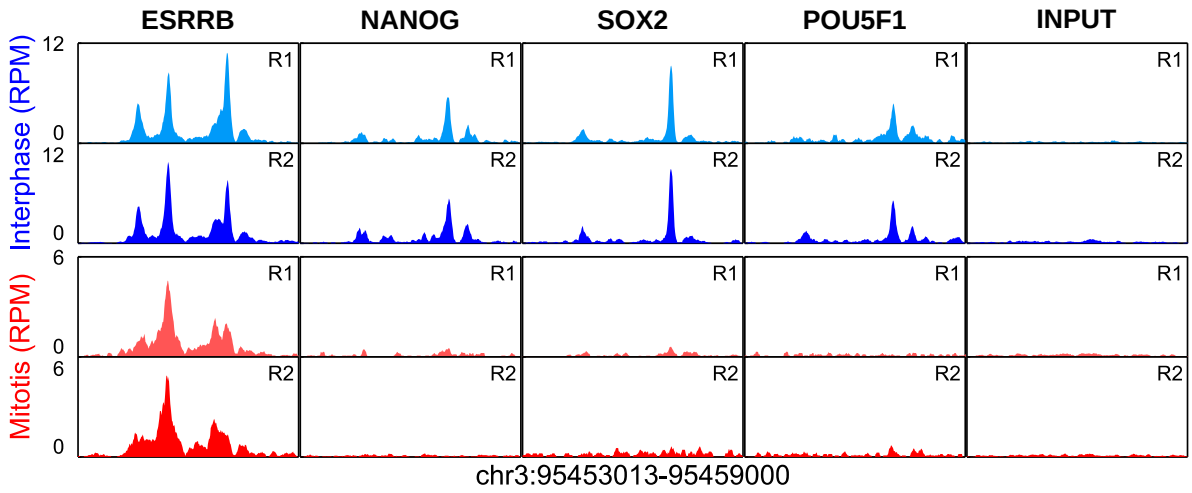

Supplemental Figure S2: Closer visualisation of a 6kb-long genomic region. Binding profiles of ESRRB, NANOG, SOX2 and POU5F1, along signal levels detected in INPUT samples (Reads per Million; RPM), in interphase (blue) or mitosis (red), obtained after fixation with DSG+FA. Two replicates are shown for each.

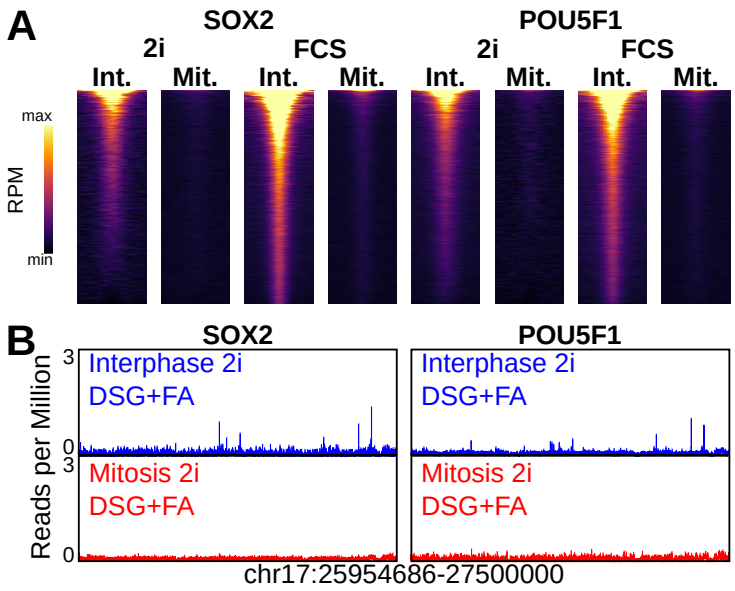

Supplemental Figure S3: POU5F1 and SOX2 binding in 2i-treated ES cells. (A) Heatmaps of ChIP-seq signal in interphase and mitosis for SOX2 and POU5F1, in cells cultured in the presence of 2 inhibitors (2i) of MEK and GSK3b or not (FCS). Binding regions are the union of peaks identified in both conditions. The heatmap (0 to 1 Reads per Million) is presented as in Fig. 4A. **(B)** Representative binding profile for SOX2 (left) or POU5F1 (right) in interphase (blue) or mitosis (red), obtained after fixation with DSG+FA in 2i treated cells; vertical scale Reads per Million. The region corresponds exactly to that shown in Figs. 1 and 2.

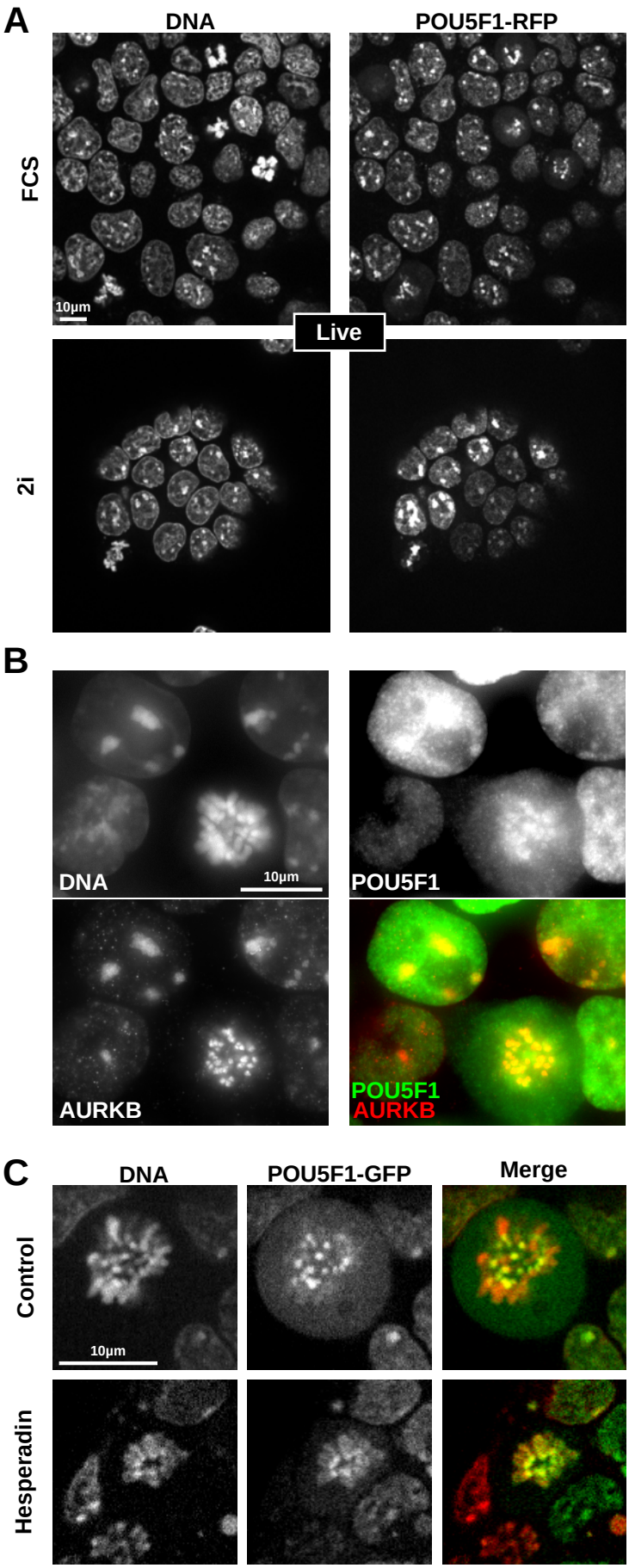

Supplemental Figure S4: Extended analysis of POU5F1 localisation. (A) Localisation of POU5F1-RFP fusion proteins expressed from one of the two endogenous *Pou5f1* alleles in live cells cultured in regular conditions (FCS/LIF medium; top) or in the presence of 2 inhibitors (2i; bottom) of MEK and GSK3b. DNA is visualised by Hoechst 33342 (red). **(B)** POU5F1 (green in the merge) and AURKB (red in the merge) immunofluorescence after fixation with DSG+FA. Note the large overlap at PCH and at centromeres in interphase and in mitosis. **(C)** Localisation of POU5F1-GFP fusion proteins in live cells cultured in the presence (bottom) or absence (top) of the AURKB inhibitor Hesperadin. DNA is visualised by Hoechst 33342 (red). Note this image corresponds exactly to that shown in Fig. 3A.

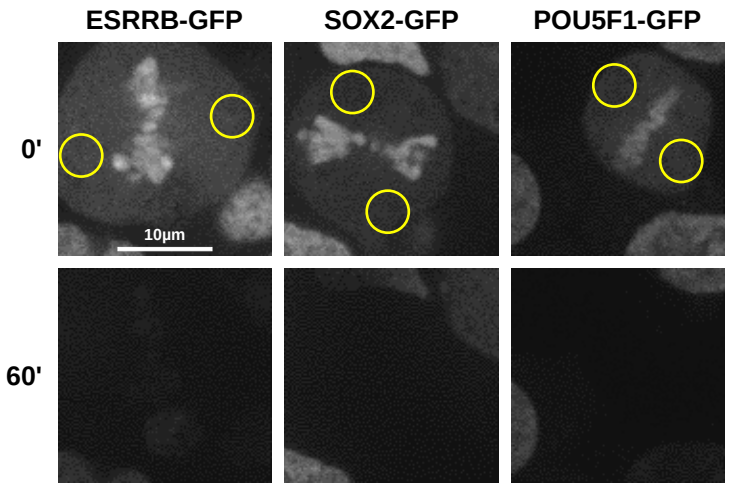

Supplemental Figure S5: Example of FLIP imaging. Representative examples of ESRRB-GFP, SOX2-GFP and POU5F1-GFP signal on mitotic chromosomes before and after 60 seconds of continuous bleaching of freely diffusing molecules outside the chromatids. The bleached areas are shown with yellow circles.

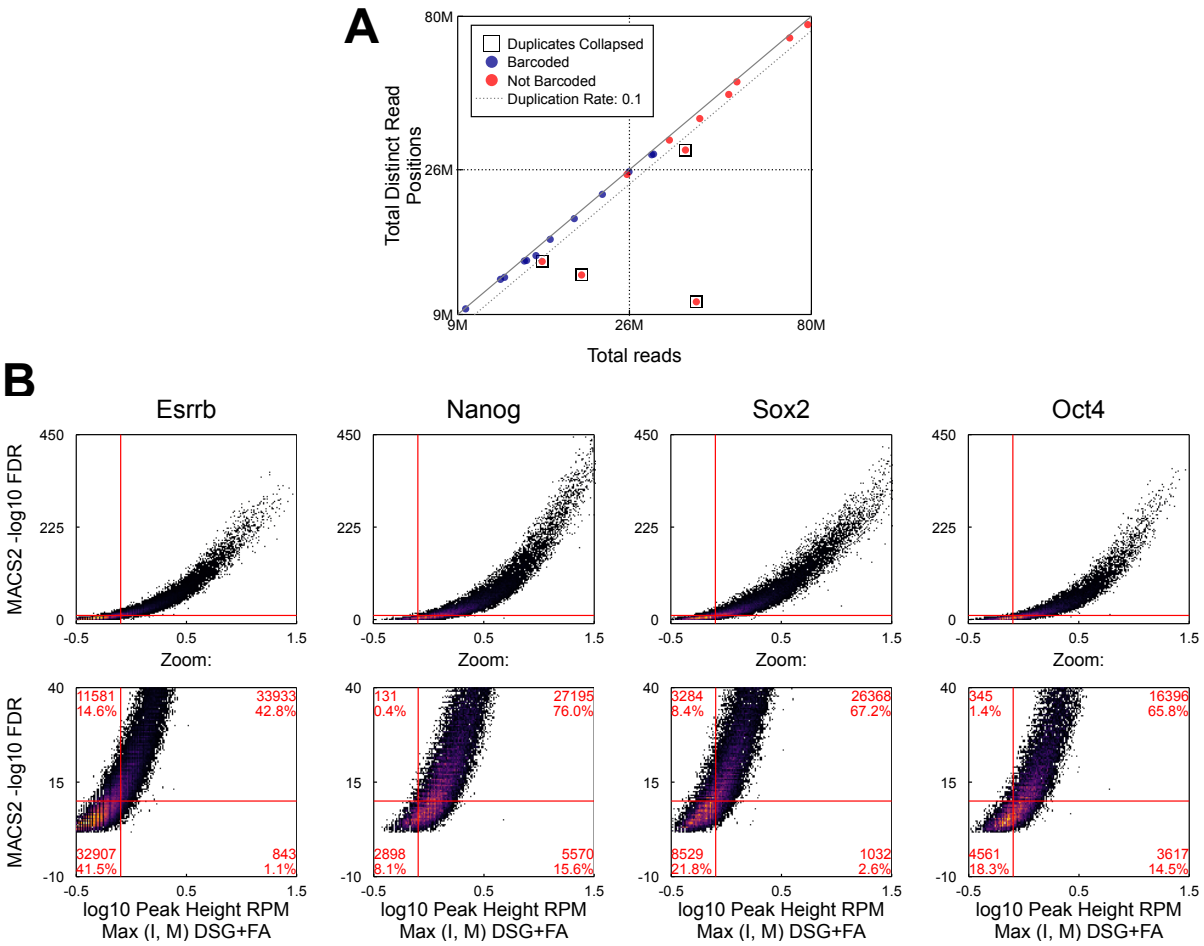

Supplemental Figure S6: Overview of TF binding sites identification. (A) For all libraries that were not constructed with random barcodes (red dots in the plot; see Supplemental Table S1 and Supplemental Methods) we collapsed duplicated reads into one only when the duplication rate in the library was above 10% (squared dots in the plot). See Supplemental Methods for details. **(B)** For all TF ChIP-seq datasets, we only considered MACS2 peaks with a height and FDR above the indicated thresholds (see Supplemental Methods for details).

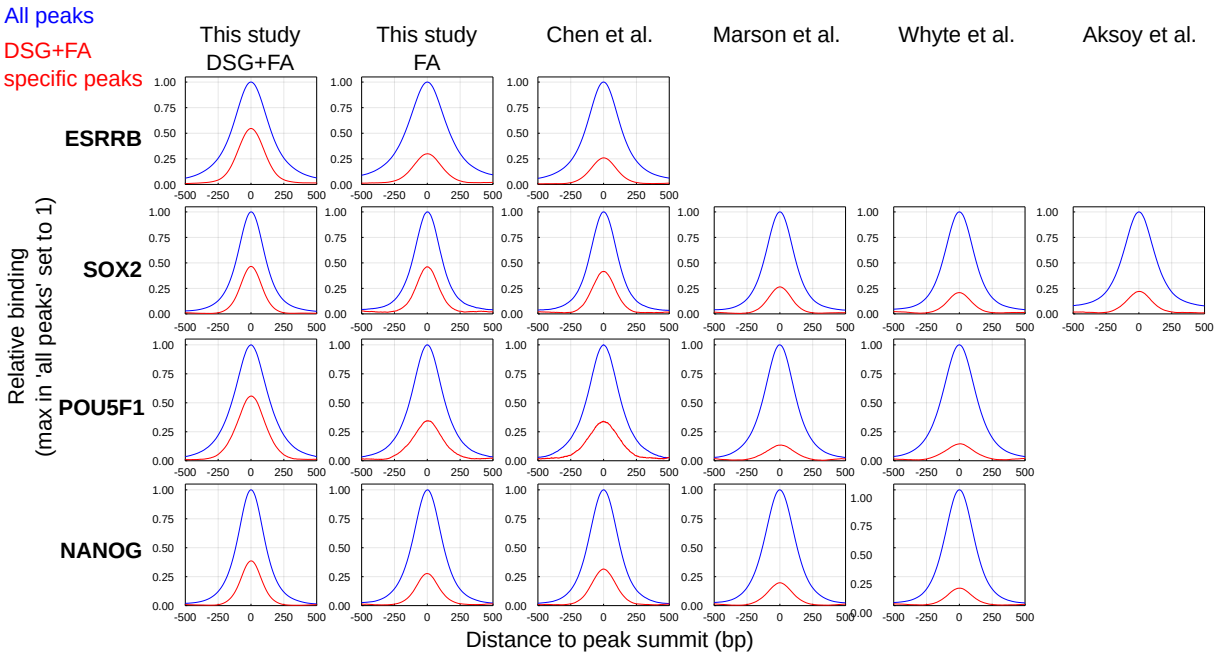

Supplemental Figure S7: Analysis of peaks specifically detected in DSG+FA. Average binding profile in interphase of ESRRB, SOX2, POU5F1 and NANOG, in this study and in public datasets. Blue line depicts all binding regions identified in this study, red depicts regions detected in DSG+FA exclusively, i.e. regions with no significant peak in any of the indicated FA datasets.

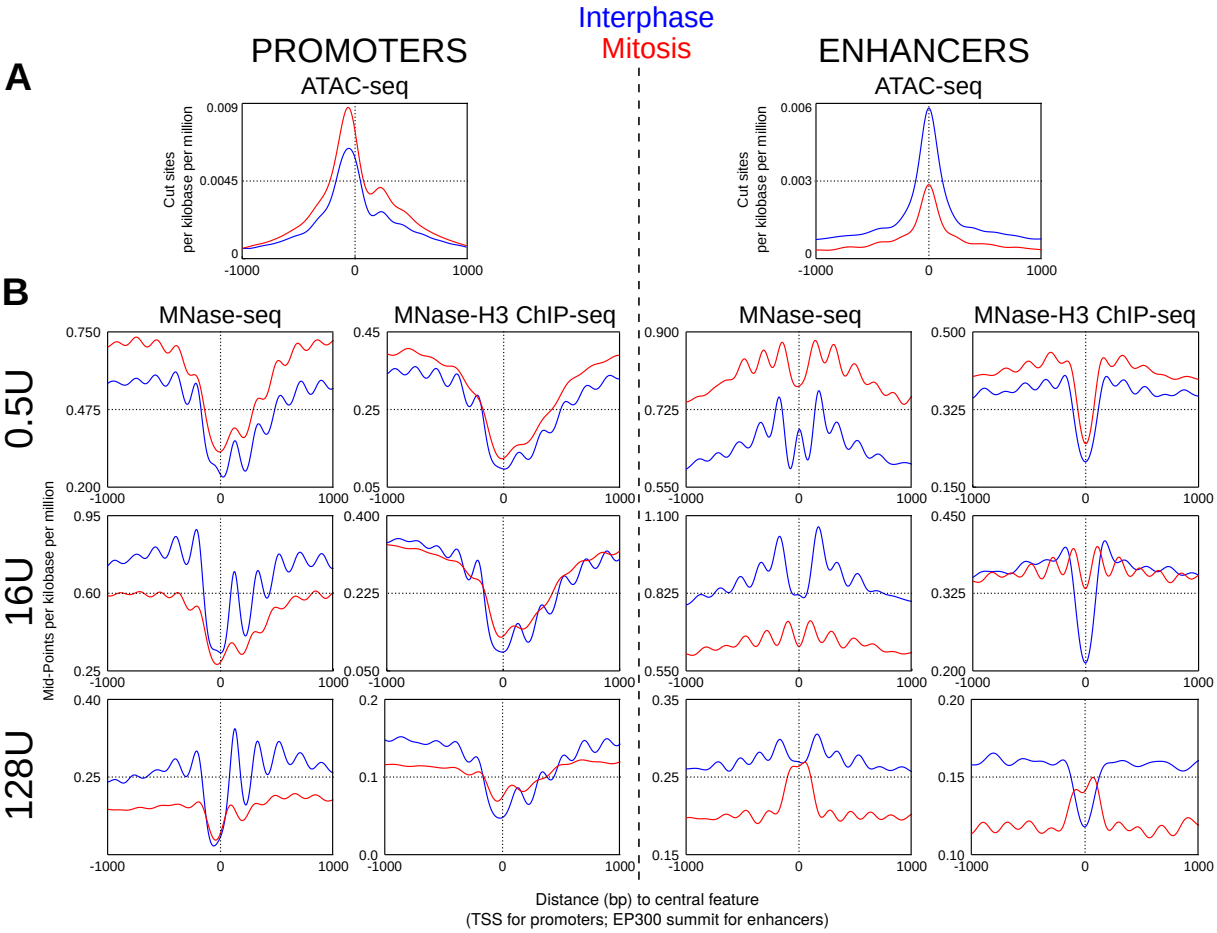

Supplemental Figure S8: Full ATAC-seq, MNase-seq and MNase-H3 ChIP-seq datasets at promoters and enhancers. (A) Chromatin accessibility at promoters (left) and enhancers (right) by ATAC-seq in interphase (blue) and mitosis (red). The Y axis shows the number of cut sites per base per million. To focus on differences in local enrichment over background, we use a minimum accessibility normalisation in Fig. 5A, D (see Supplemental Methods for details). **(B)** Nucleosome positioning at promoters (left) and enhancers (right), established by increased digestion with MNase, as indicated on the left (0.5U; 16U; 128U), in interphase (blue) and mitosis (red). The Y axis shows the number of midpoints of nucleosome-sized fragments (140-200bp) per base, per kilobase and per million fragments. Lines are Gaussian process regression of midpoint data. To generate the corresponding Fig. 5B, E, we used a z-score transformation (see Supplemental Methods for details) to compare differences in positioning rather than in magnitude. The X axis shows the genomic position centred on TSS for promoters and EP300 summits for enhancers.

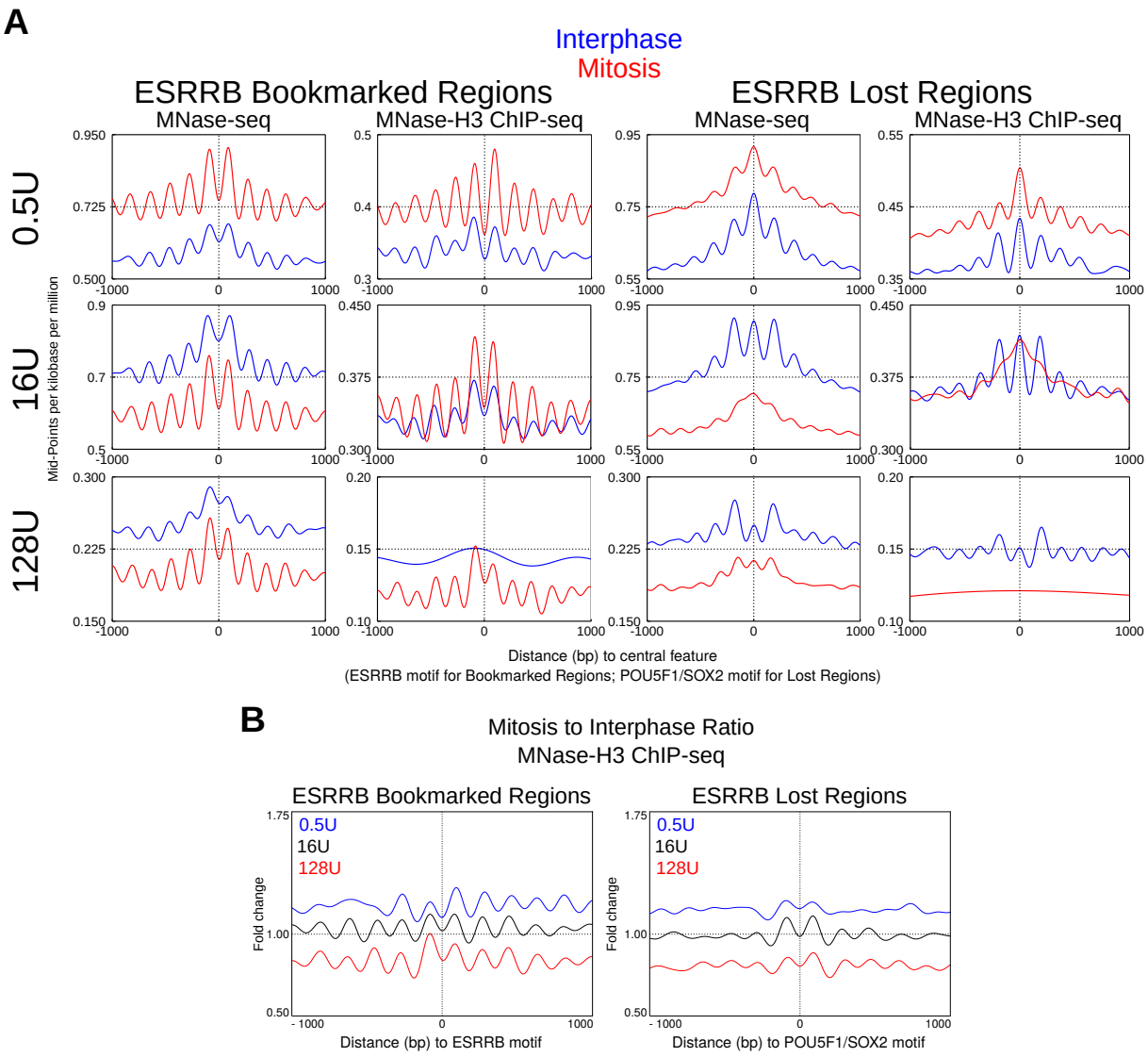

Supplemental Figure S9: Full MNase and MNase-H3 ChIP-seq datasets at ESRRB binding regions. (A) Nucleosome positioning at bookmarked (left) and not-bookmarked (Lost; right) ESRRB binding regions, established by increased digestion with MNase, as indicated on the left (0.5U; 16U; 128U), in interphase (blue) and mitosis (red). The Y axis shows the number of midpoints of nucleosome-sized fragments (140-200bp) per base, per kilobase and per million fragments. Lines are Gaussian process regression of midpoint data. The X axis shows the genomic position centred on ESRRB motifs for bookmarked regions and on POU5F1/SOX2 motifs for lost regions. **(B)** Mitosis over interphase ratio of MNase-H3 ChIP-seq signal for nucleosomal fragments for MNase digestions with 0.5U (blue), 16U (black) and 128U (red) of enzyme, at bookmarked (left) and lost (right) regions.

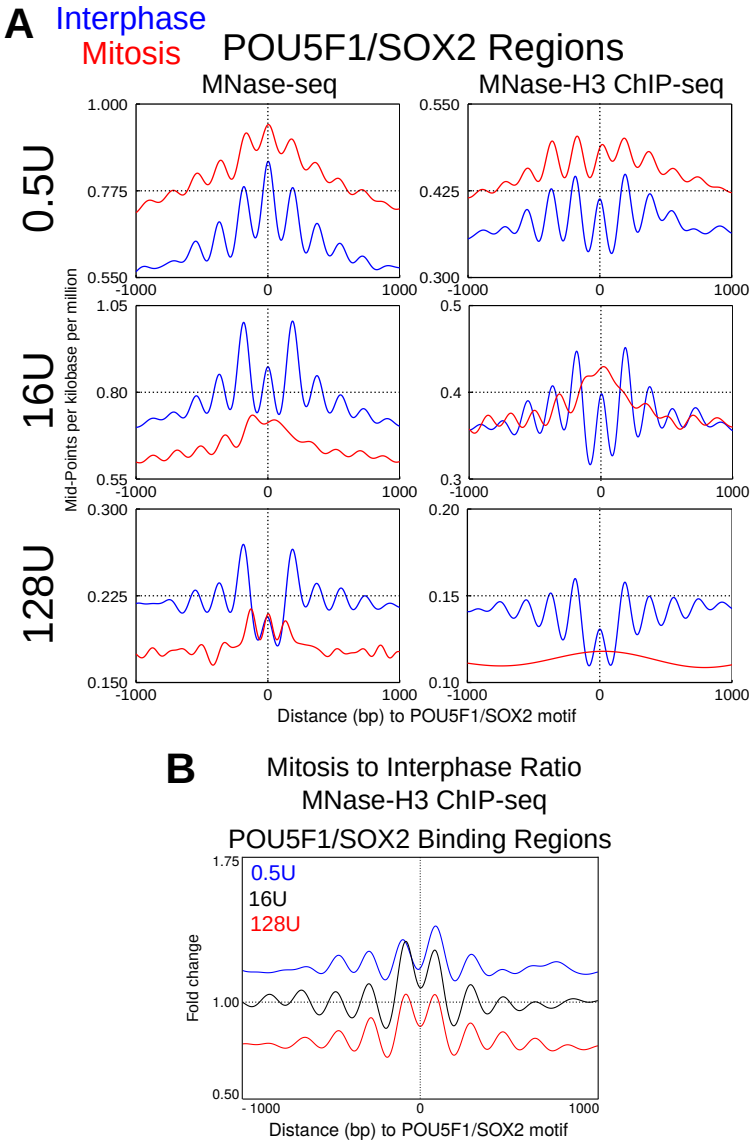

Supplemental Figure S10: Full MNase and MNase-H3 ChIP-seq datasets at POU5F1/SOX2 binding regions. (A) Nucleosome positioning at POU5F1/SOX2 binding regions, established by increased digestion with MNase, as indicated on the left (0.5U; 16U; 128U), in interphase (blue) and mitosis (red). The Y axis shows the number of midpoints of nucleosome-sized fragments (140-200bp) per base, per kilobase and per million fragments. Lines are Gaussian process regression of midpoint data. The X axis shows the genomic position centred on POU5F1/SOX2 motifs **(B)** Mitosis over interphase ratio of MNase-H3 ChIP-seq signal for nucleosomal fragments for MNase digestions with 0.5U (blue), 16U (black) and 128U (red) of enzyme, at bookmarked (left) and lost (right) regions.

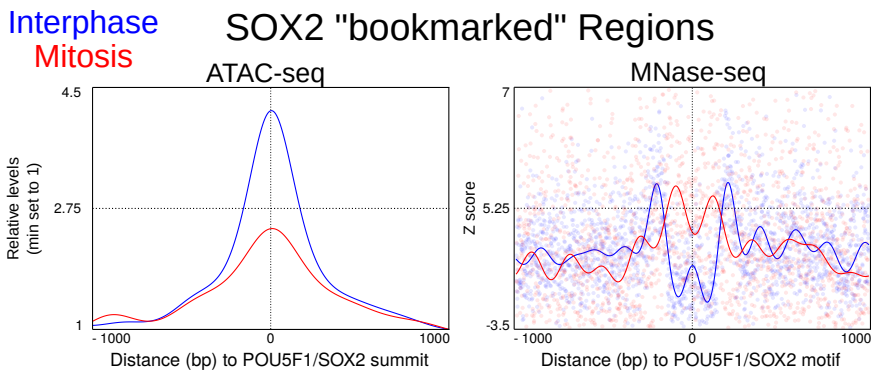

Supplemental Figure S11: Chromatin analysis of pseudo-bookmarked SOX2 binding regions. Left: Accessibility measured by cut sites of 0-100 bp ATAC-seq fragments at SOX2 putative bookmarked sites in interphase and mitosis, centred on SOX2 peak summits. Right: Nucleosome positioning measured by MNase-seq nucleosomal size fragments (140-200 bp) after digestion with 16U at SOX2 putative bookmarked sites centred on POU5F1/SOX2 motif. Vertical scale gives z-score.

Transcription factor activity and nucleosome organisation in mitosis

Festuccia, N., Owens, N., et al.

SUPPLEMENTAL METHODS

Contents:

1/ Animals and embryos production.

All experiments were conducted according to the French and European regulations on care and protection of laboratory animals (EC Directive 86/609, French Law 2001-486 issued on June 6, 2001). Embryos were collected from (CD1-Crl) females mated with males of the same genotype, purchased from Charles River Laboratories, France. Blastocysts were collected from females at E3.25 in EmbryoMax M2 Medium (Millipore Bioscience, Cat# MR-015D) and cultured for five hours in EmbryoMax KSOM (Millipore Bioscience, Cat# MR-121D) with 10µM MG132 (Sigma, Cat# M7449-200UL) to prevent blastomere mitotic exit.

2/ Culture and Generation of ES cells.

2a/ General culture conditions.

ES cells were cultured on 0.1% gelatine (SIGMA, Cat# G1890-100G) in DMEM + GlutaMax-I (Gibco, Cat# 31966-021), 10% FCS (Gibco, Cat# 10270-098), 100 µM 2-mercaptoethanol (Gibco, Cat# 31350-010), 1× MEM non-essential amino acids (Gibco, Cat# 1140-035) and 10 ng×ml^{-1} recombinant LIF (MILTENYI BIOTEC, Cat# 130-099-895). Cells were passaged 1:10 every 2–3 days. When indicated, cells were grown in 2i-containing medium (1 µM PD0325901 and 3 µM CHIR99021; Axon Medchem Bv) - either directly supplemented to FCS/LIF medium (for chromatin studies), or in serum-free medium: 0.5× DMEM/F12 (Gibco, Cat# 31331093), 0.5×Neurobasal (Gibco, Cat# 21103049), 0.5% N2 supplement 100× (Gibco, Cat# 17502048), 1% B27 supplement 50× (Gibco, Cat# 17504044), 10µg/mL Insulin (Sigma, Cat# I1882-100MG), 2 mM L-Glutamine (Invitrogen, Cat# 91139), 0.05% BSA (Sigma, Cat# A3311-10G), 100 µM 2-mercaptoethanol (Gibco, Cat# 31350-010), 10 ng/ml recombinant LIF (MILTENYI BIOTEC, Cat# 130-099-895).

2b/ Derivation of Esrrb-GFP, Nanog-GFP and POU5F1-GFP ESCs.

E14Tg2a cells were stably transfected with CAG-*Nanog*-GFP-IRES-puromycin^R or CAG-*Pou5f1*-GFP-IRES-puromycin^R transgenes. ECKOiE cells (Festuccia et al. 2016) were stably transfected with CAG-*Esrrb*-GFP-IRES-puromycin^R and selected by culture in the absence of doxycycline. For all cell lines, clones expressing low, comparable and homogeneous levels of the fluorescent proteins were selected.

2c/ Derivation of Ccna-GFP Sox2-AID ES cells.

E14Tg2a expressing a Ccna-GFP fusion protein (Festuccia et al. 2016) were lipofected with 3µg of a linearised targeting vector designed to insert a 5×Gly linker –Auxin inducible degradation domain-IRES Blasticidin^R cassette at stop codon of *Sox2* and 1µg of pU6_CBh-Cas9-T2A-mCherry (Addgene no. 64324) driving expression of the gRNA 3'- CAGGGGCAGTGTGCCGTTAA -5'. 48 hours later selection was added and after 2 weeks single colonies were picked, expanded, and correctly targeted cells identified by PCR on genomic DNA and sequencing. ES lines homozygous for the desired recombination product were further lipofected with 3µg of a linearised targeting vector designed to insert a CAG-OsTir-T2a-Neomycin^R cassette at the TIGRE locus and 1µg of pU6_CBh-Cas9-T2A-mCherry (Addgene no. 64324) driving expression of the gRNA 3'- ACTGCCATAACACCTAACTT-5'. 48 hours later selection was added and after 2

weeks single colonies were picked, expanded, and correctly targeted cells identified by PCR on genomic DNA and sequencing. One heterozygous line, Ccna-GFP *Sox2*-AID c1.2, was used for the experiments described.

3/ Imaging.

3a/ Culture conditions for all imaging experiments.

Cells were plated on IBIDI hitreat plates coated overnight with poly-L-ornithine 0.01% (Sigma, Cat# P4957) at 4 °C, washed and coated 2 h with laminin (Millipore, Cat# CC095) 10 $\mu g \times ml^{-1}$ in PBS.

3b/ Immunofluorescence on fixed cells.

Fixation: we had previously observed that standard karyotype protocols using acetic acid and methanol allowed the visualisation of mitotic chromosome coating by ESRRB (Festuccia et al. 2016). However, these conditions did not enable us to perform ChIP appropriately (data not shown). Therefore, we tried several combinations of acetic acid, ethanol or methanol, mixed at different ratios with formaldehyde (FA), without success – only very partial retention of ESRRB on mitotic chromosomes was observed. Only the use of disuccinimidyl glutarate (DSG) or glyoxal allowed the fixation of TF binding to the chromatin in mitotic cells. The following steps were performed after washing cells growing in IBIDI dishes twice with PBS:

- FA: Cells were incubated for 10 min in 1 ml PBS 1% formaldehyde (Thermo, Cat# 28908) at room temperature.
- DSG: Cells were crosslinked in 1 ml of freshly prepared PBS-DSG 2 mM at pH 7.0 (Sigma, Cat# 80424-5 mg) for 50 min at room temperature. To prepare DSG, 5mg were first dissolved in 30.6µl of DMSO, and then 4µl of the solution added directly into 1ml PBS at room temperature while vortexing.
- DSG+FA only: After washing DSG-fixed cells in PBS, cells were incubated for 10 min in 2 ml PBS 1% formaldehyde (Thermo, Cat# 28908) at room temperature.
- Glyoxal: Fresh fixative solution was prepared before each experiment mixing 2.835 ml H2O, 0.789 ml ethanol, 0.313 ml glyoxal 40% stock (Sigma, Cat# 128465), 0.03 ml acetic acid. The solution was brought to pH 5.0 with NaOH. Cells were incubated for 30 min in the fixative solution on ice.
- Glyoxal+FA only: Glyoxal-fixed cells were washed with PBS and incubated for 10 min in 1 ml PBS 1% formaldehyde (Thermo, Cat# 28908) at room temperature.

Staining: all cells were washed twice in PBS and permeabilised with PBS/0.1% v/v Triton X-100 supplemented with 3% of donkey serum (Sigma, Cat# D9663) for 15 min at room temperature. Primary antibodies (diluted in PBS with donkey serum 3%) were applied 2 hours at room temperature or overnight at 4°C in a volume of 1ml per dish. After three washes in PBS/0.1% Triton X-100, secondary antibodies (2µg/ml in PBS with donkey serum 3%) were applied for 2 hours at room temperature. Cells were washed three times in PBS/0.1% v/v Triton X-100, nuclei counterstained with 4',6-diamidino-2-phenylindole (DAPI; Sigma, Cat# D9542), and imaged with a LSM800 Zeiss microscope using a 64× oil-immersion objective.
Primary antibodies were used at the following concentrations:

- 1:500 anti-NANOG (E-bioscience, Cat #14-5761-80)
- 0.4µg/ml anti-POU5F1 (Santa Cruz Biotechnology, Cat #sc-5279)
- 0.4µg/ml anti-SOX2 (Santa Cruz Biotechnology, Cat #sc-17320)
- 2µg/ml anti-ESRRB (Perseus Proteomics, Cat #PP-H6705-00)

Secondary antibodies: Alexa Fluor 594 AffiniPure Donkey Anti-Rabbit IgG (H+L) (Jackson ImmunoResearch, Cat #711-585-152); Alexa Fluor 488 AffiniPure Donkey Anti-Mouse IgG (H+L) (Jackson ImmunoResearch, Cat #715-545-150); Alexa Fluor 488 AffiniPure Donkey Anti-Goat IgG (H+L) (Jackson ImmunoResearch, Cat #705-546-147); Alexa Fluor 488 AffiniPure Donkey Anti-Rat IgG (H+L) (Jackson ImmunoResearch, Cat# 712-545-150).

ES cells treated with hesperidin: E14Tg2a cells growing in IBIDI plates were treated with nocodazole 50 ng×ml^{-1} for 4 h and 500nM hesperadin (Selleck Chemicals, S1529) for 15min prior to fixation with DSG+FA and staining as described above. Primary antibodies: goat anti-POU5F1 (Santa Cruz, sc8628; 1:500) and rabbit anti-AURKB (Abcam, ab2254; 1:500). Secondary antibodies AffiniPure donkey anti-rabbit and anti-goat (711-545-152 Alexa 594 and 705-585-147 Alexa 488 respectively, 1:500, Jackson ImmunoResearch). Images of 500 nm z-steps were acquired on a Nikon Eclipse Ti inverted microscope equipped with a 63x oil-immersion objective (N.A. 1.4), a Hamamatsu ORCA Flash 4.0LT camera using the NIS Elements 4.3 software.

3c/ Spinning-disc live imaging:

Esrrb-GFP, *Nanog*-GFP, *Sox2*-GFP, *Pou5f1*-GFP and *Pou5f1*-RFP ES cells growing in FCS+LIF in IBIDI plates were switched to phenol red-free medium (Gibco, 31053-028). Cells were incubated with 500 nM Hoechst-33342 for 20 min before imaging. During imaging the cells were kept at 37 °C in a humidified atmosphere (7% CO_2). Image z-stacks were acquired every 600 nm with a 63× oil immersion objective on a Zeiss AxioObserver Z1 microscope equipped with a Yokogawa CSUX1 spinning-disk confocal scanner, a Hamamatsu EMCCD ImageEM X2 camera using the Volocity acquisition software.

3d/ Spinning-disc live imaging for FRAP:

Cells were transferred to red-phenol-free medium before imaging and kept at 37 °C in a humidified atmosphere (7% CO_2) during the entire duration of the experiments. Images were acquired using a 63× oil immersion objective on a Zeiss AxioObserver Z1 microscope equipped with Yokogawa CSUX1 spinning-disc confocal set-up, a Hamamatsu EMCCD ImageEM X2 camera and Volocity imaging software. For FRAP, 5 frames were acquired before bleaching (20 ms pulse using a 488 nm laser, spot of minimal size) and then recovery was imaged for 1 min or 30 seconds (1 image each 110 ms) for interphase and mitosis respectively (pixel size 0.2 µm). For FLIP, before each acquisition, two areas of 10 × 10 pixels (2 × 2 µm) located at the opposite end of the cell being analysed were bleached using a 488 mm laser. Bleaching and acquisition cycles were repeated at maximum speed (310 ms), for a total time of 190 seconds. For FRAP, fluorescence recovery was analysed in Matlab as described previously (Mueller et al. 2012), with one modification: the bleached region was located automatically by subtracting the first pre-bleach image from the last post-bleach image and calculating the two-dimensional convolution (conv2 function) of this image with a circle of the typical size of a bleach spot.

3e/ Embryo immunofluorescence.

Embryos were fixed for 24 hours at 4°C with 2 mM DSG (Sigma Aldrich Cat# 80424-5MG) in PBS and then for 20 min at room temperature in 4% formaldehyde (Euromedex Cat# 15714). Incubation with primary and secondary antibodies was performed in PBS 0.1% Triton X-100, 10% donkey serum. The following antibodies were used: anti-NANOG (1:100; rabbit CosmoBio Cat# REC-RCAB0002PF), anti-ESRRB clone H6705 (1 :100; Perseus Proteomics, Cat# PP-H6705-00), Alexa 488-nm anti-rabbit (1:300; Invitrogen Cat# A21206) and Alexa 647-nm anti-mouse antibody (1:300; Invitrogen Cat# A31571). Embryos were incubated at room temperature for 2 hours with primary antibodies and for 1 hour with secondary antibodies. Nuclei were counterstained with Hoechst 33342 (1.6 µM; Sigma Aldrich, B2261-25MG), and embryos were placed individually in glass bottom microwell dishes (MatTek Corporation) in PBS. Fluorescent images were obtained using a confocal laser-scanning microscope (LSM800; Zeiss) with the objective Plan-apochromat 20 × /NA 0.8, speed 6, pinhole 1 airy unit, and laser intensities suited for optical section thickness of 2 µm. Images show one embryo out of the four of the same experiment which harboured mitotic cells. The experiment was performed four times independently.

4/ Chromatin studies.

4a/ Preparation of mitotic populations.

E14tg2a cells were grown to 70–80% confluency in T150 flasks. Vigorous shake-off was performed to detach debris, dying cells or poorly attached cells colonies, medium discarded and flasks washed twice in PBS. After 4-5 h in medium containing 50 ng×ml^{-1} nocodazole (Sigma, Cat# M1404), flasks were gently washed with PBS. Gentle shake-off was performed in 10 ml of medium, monitoring the process under a microscope to avoid detaching clumps of cells in interphase. The cell suspension was filtered through a 10µm filter (pluriSelect, Cat# 43-50010-03) by gravity and cells spun down. Typically, around 10^7 cells were obtained from each preparation. Purity of mitotic preparations was systematically checked under a fluorescence microscope after fixation, cytospinning and DAPI staining. Preparations with more than 5% contamination from interphase were discarded.

4b/ Chromatin preparation for TF-binding analysis.

Fixation DSG+FA. 10^7 ES cells were crosslinked in 2 ml of freshly prepared PBS-DSG 2 mM at pH 7.0 (Sigma, Cat# 80424-5 mg) for 50 min at room temperature with occasional shaking. After pelleting and washing once in PBS, cells were incubated for 10 min in 2 ml PBS 1% formaldehyde (Thermo, Cat# 28908). Crosslinking was stopped with 0.125 M glycine for 5 min at room temperature. Cells were pelleted and washed with ice-cold PBS.

Fixation FA: ES cells (10^7) were resuspended in 3 ml of pre-warmed DMEM/FCS/LIF and crosslinked for 10 min at room temperature adding 1% formaldehyde (Thermo, Cat# 28908). Crosslinking was stopped with 0.125 M glycine for 5 min at room temperature. Cells were pelleted and washed with ice-cold PBS.

Chromatin preparation: For interphase preparation exclusively, cells were resuspended in 2 ml of swelling buffer (25 mM Hepes pH 7.95, 10 mM KCl, 10 mM EDTA) freshly supplemented

with 1× protease inhibitor cocktail (PIC-Roche, Cat# 04 693 116 001) and 0.5% IGEPAL. After 30 min on ice, the suspension was passed 40 times in a dounce homogenizer (only for asynchronous populations). For mitosis and interphase preparations: cells were centrifuged and resuspended in 300 µl of TSE150 (0.1% SDS, 1% Triton X-100, 2 mM EDTA, 20 mM Tris-HCl pH8, 150 mM NaCl) buffer, freshly supplemented with 1× PIC. Samples were sonicated in 1.5 ml tubes (Diagenode) using a Bioruptor Pico (Diagenode) for 7 cycles divided into 30 s ON–30 s OFF sub-cycles at maximum power, in circulating ice-cold water. After centrifugation (30 min, full speed, 4 °C), the supernatant was either used immediately for immunoprecipitation or stored at −80 °C until use, generally within the month. Five microliters were used to quantify the chromatin concentration and check DNA size (typically 200–350 bp).

4c/ Chromatin immunoprecipitation (ChIP).

For ChIP-qPCR and ChIP-Seq experiments, chromatin from $2x10^6$ and 10^7 cells was used, respectively. Chromatin was pre-cleared for 3 hours rotating on-wheel at 4 °C in 300 µl of TSE150 containing 50 µl of protein G Sepharose beads (Sigma, Cat# P3296-5 ML) 50% slurry, previously blocked with BSA (500 µg×ml^{-1}; Roche, Cat# 5931665103) and yeast tRNA (1 µg×ml^{-1}; Invitrogen, Cat# AM7119). Immunoprecipitations with anti-ESRRB mouse monoclonal (1µg per $2x10^6$cells, 5 µg per 10^7 cells; Perseus Proteomics, Cat# H6-705-00), anti-NANOG rabbit polyclonal (0.6 µg per $2x10^6$cells, 3 µg per 10^7 cells; Cosmobio, Cat# REC-RCAB001P); anti-POU5F1 goat polyclonal (0.6 µg per $2x10^6$cells, 3 µg per 10^7 cells; Santa Cruz Biotechnology, Cat # sc-5279); anti-SOX2 goat polyclonal (0.6 µg per $2x10^6$cells, 3 µg per 10^7 cells; Santa Cruz Biotechnology, Cat # sc- 17320), were performed overnight rotating on-wheel at 4 °C in 500 µl of TSE150. Twenty microliters were set apart for input DNA extraction and precipitation. Twenty-five microliters of blocked protein G beads 50% slurry was added for 4 h rotating on-wheel at 4 °C. Beads were pelleted and washed for 5 min rotating on-wheel at room temperature with 1 ml of buffer in the following order: 3 × TSE150, 1 × TSE500 (as TSE150 but 500 mM NaCl), 1× washing buffer (10 mM Tris-HCl pH8, 0.25M LiCl, 0.5% NP-40, 0.5% Na-deoxycholate, 1 mM EDTA), and 2 × TE (10 mM Tris-HCl pH8, 1 mM EDTA). Elution was performed in 100 µl of elution buffer (1% SDS, 10 mM EDTA, 50 mM Tris-HCl pH 8) for 15 min at 65 °C after vigorous vortexing. Eluates were collected after centrifugation and beads rinsed in 150 µl of TE-SDS1%. After centrifugation, the supernatant was pooled with the corresponding first eluate. For both immunoprecipitated and input chromatin, the crosslinking was reversed overnight at 65 °C, followed by proteinase K treatment, phenol/chloroform extraction and ethanol precipitation.

4d/ MNase-seq and H3 ChIP-seq on MNase digested chromatin.

10^7 ESCs were resuspended in 3 ml of pre-warmed DMEM/FCS/LIF and crosslinked for 10 min at room temperature adding 1% formaldehyde (Thermo, Cat# 28908). Crosslinking was stopped with 0.125 M glycine for 5 min at room temperature. Cells were pelleted and washed with ice-cold PBS. 2.5 x 10^6 cells were resuspended in 500µl of MNase buffer (50mM Tris-HCl pH8, 1mM CaCl2, 0.2% Triton X-100) supplemented with protease inhibitor cocktail (PIC-Roche, Cat# 04 693 116 001). Cells were pre-incubated for 10 min at 37°C and ½ U, 16 U or 128 U of MNase (Expressed in KUntiz, 1 Kunitz is equivalent to 10 gel units, NEB Cat# M0247S) added to the reaction. Cells were incubated for further 10 min at 37°C, inverting the tubes occasionally. The reaction was stopped on ice by adding 500ul of 2 × STOP buffer (2% Triton

X-100, 0.2% SDS, 300mM NaCl, 10mM EDTA). Tubes were left rotating overnight on a wheel to allow diffusion of the digested fragments. The cell suspension was spun down and the supernatant stored at -80°C.

MNase-seq: 250 µl (for 0.5U digestion conditions) or 25µl (for 16U and 128U digestion conditions) of chromatin were brought to a final volume of 250µl and 1% SDS concentration. Samples were incubated over night at 65°C to revert the crosslinking. The next day, 250µl of TE and 5µl of 20 mg/ml Proteinase K (Eurobio, Cat# GEXPRK) were added and samples incubate 2 hours at 37°C. DNA was phenol/chloroform extracted and ethanol precipitated. Samples were resuspended in 50µl of TE and 2 µl of RNase (Roche, Cat# 11119915001) were added. After 30 minutes incubation at 37°C, DNA was purified with SPRI beads as described (see The Library Preparation section), adding 90µl of beads and 50 µl isopropanol, and eluted in 40µl of water. 1µl was used to measure the DNA concentration with a Qubit 3 (Invitrogen, Cat# Q33218). 1 ng of DNA was used to check fragment size with a D1000 High Sensitivity Screentape and appropriate reagents (Agilent, Cat# 5067-5584, Cat# 5067-5585) on an Agilent 2200 Tapestation. In case genomic DNA of high molecular weight was observed, the samples were absorbed on SPRI beads, using a 0.5 ×SPRI beads/sample ratio, beads discarded, and SPRI beads added to the supernatant to reach a 1.8x bead/sample ratio. MNase libraries were prepared as described (see the Library Preparation section) using a starting amount of 10-20ng.

H3 ChIP-seq: 250 µl (for ½ U digestion conditions) or 50µl (for 16U and 128U digestion conditions) of chromatin were brought to a final volume of 500µl with TSE150 (0.1% SDS, 1% Triton X-100, 2 mM EDTA, 20 mM Tris-HCl pH8, 150 mM NaCl), freshly supplemented with protease inhibitor cocktail (PIC-Roche, Cat# 04 693 116 001). ChIP was performed as described (see section 4c), using 5 µg of anti-Histone H3 rabbit polyclonal (Abcam, Cat# ab1791).

4e/ ATAC-Seq.

For each experiment $5x10^4$ cells were used. Cells were harvested, counted, washed once with ice-cold PBS and spun down. Supernatants were completely removed and pellets were placed on ice. Each pellet was resuspended in 25 µl TD buffer (2× reaction buffer from Nextera kit; Illumina, Cat# FC-121-1030). After the addition of 2.5 µl of transposase TDE1 (Nextera Tn5 Transposase from Nextera kit; Illumina, Cat# FC-121-1030) and 22.5 µl nuclease free water, reactions were mixed and incubated for 30 min at 37°C in gentle agitation. Reactions were stopped by adding the appropriate volume of Binding Buffer (Qiagen MinElute PCR Kit) and the DNA was purified using the Qiagen MinElute PCR Kit according to manufacturer's protocol. The purified DNA, eluted in 10 µl, was either stored at -20°C or used directly for library preparation.

5/ Library Preparations.

5a/ SPRI Bead preparation.

1 ml Sera-Mag™ Magnetic SpeedBeads™, carboxylated, 1 µm, 3 EDAC/PA5 (GE Healthcare Life Sciences, Cat# 65152105050250) were washed 3 times with a TE-Tween solution (10 mM Tris HCl pH 8, 1 mM EDTA, 0.05% Tween 20, pH 8.0) and resuspended in TE-Tween-20% PEG 8000 solution (10 mM Tris HCl pH 8, 1 mM EDTA, 0.05% Tween 20, pH 8.0).

5b/ Library preparation for ATAC.

Reactions were prepared mixing 10 µl transposed DNA, 2.5 µl 25 µM primer Ad1.noMX, 2.5 µl 25 µM primer Ad2 from (Buenrostro et al. 2013), 9 µl Nuclease Free Water, 1 µl of a 1:8 dilution of Quant-iT Picogreen dye (Invitrogen, Cat# P11496) and 25µl of KAPA HiFi HotStart 2× Master Mix (Kapa Bioscience Cat# KK2502). Reaction mix was transferred to qPCR plates and amplification was carried out under the following conditions: Pre-amplification: 1 cycle: 5' at 72°C; 30" at 98°C; 5 cycles: 10" at 98°C; 30" at 63°C; 1' at 72°C; Amplification: 1 cycle: 30" at 98°C; 11/12 cycles: 10" at 98°C; 30" at 63°C; 1' at 72°C. After amplification libraries were purified with SPRI beads, using a sample to bead ratio of 1: 1.4. 1µl was used to measure the DNA concentration with a Qubit 3 and the provided reagents (Invitrogen, Cat# Q33218). 1 ng of DNA was used to check fragment size with a D1000 High Sensitivity Screentape and appropriate reagents (Agilent, Cat# 5067-5584, Cat# 5067-5585) on an Agilent 2200 Tapestation. Libraries were sequenced (PE150) by Novogene Co. Ltd.

5c/ General library preparation.

End repair: Precipitated DNA was resuspended in 37.5µl of water and mixed with 2µl of 10mM dNTPs, 5µl of NEB T4 ligase buffer, 2.5µl of NEB T4 polymerase (Cat# M0203L), 0.5µl of NEB Klenow polymerase (Cat# M0210L) and 2.5µl of NEB T4 PNK (Cat# M0201L). Samples were incubated 30 min at 20^{o}C in a thermocycler. DNA was purified with SPRI beads: 90µl of SPRI bead suspension and 50µl isopropanol were added and samples transferred to a 96 well plate. After incubating for 5 min, the plate was put on a 96S Super Ring Magnet (Alpaqua, Cat# A001322), beads were allowed to separate completely, and the supernatant removed without disrupting the bead pellet. Beads were washed twice with 200µl of 70% Ethanol and the supernatant completely removed. DNA was eluted in 21µl of water.

A-Tailing: 20µl of sample were mixed with 2.5µl of NEB Buffer #2, 1µl of 5mM dATP, 1.5µl of NEB Klenow 3'-5' exo minus (Cat# M0212L), and incubated at 37^{o}C for 30min in a thermocycler. DNA was purified with SPRI beads as before, but using a volume of 45µl of beads and 25µl isopropanol. DNA was eluted in 20µl of water.

Adaptor ligation: 19µl of sample were mixed with 2.5µl of NEB T4 ligase buffer, 1.25µl of a 0.2µM solution of annealed adapters, and 2.5µl of NEB concentrated T4 ligase (Cat# M0202M) and incubated overnight at 16^{o}C. DNA was purified with SPRI beads as before, but using a volume of 35µl of beads and no isopropanol, eluting in 20 µl of water. Adaptors were designed in house. 22.5µl each of 40µM ssDNA Barcoded and Universal adaptor solutions were mixed with 5µl of NEB buffer 2, and annealed in a thermocycler.
Barcoded adaptor:
5'P-GATCGGAAGAGCACACGTCTGAACTCCAGTCAC-IIIIII-NNNNNNNN-ATCTCGTATGCCGTCTTCTGCTTG.
5'P indicates the presence of a 5'phosphate group. IIIIII represent the six base index nucleotides, and NNNNNNNN a stretch of 8 random nucleotides used for single molecule barcoding.
Universal adapter:
AATGATACGGCGACCACCGAGATCTACACTCTTTCCCTACACGACGCTCTTCCGATC*T.
* indicates the presence of a phosphorothioate bond between the last C and T.

Library amplification: 19.5 µl of sample were mixed with 1µl of a 1:10 dilution of Quant-iT Picogreen dye (Invitrogen, Cat# P11496), 25µl of KAPA HiFi HotStart 2× master Mix (Kapa Bioscience Cat# KK2502), 1µl of 10µM PCR 1.0 and 1µl of PCR 2.0 primers (See below).The amplification mix was distributed in two wells of a LightCycler 384 plate (Roche, Cat# 4729749001) and on a LightCycler 480 II instrument (Roche, Cat# 05015243001) using the following program: 1' at 98°C; N cycles: 10" at 98°C; 20" at 64°C; 45" at 72°C. The number of cycles N was determined on real time by monitoring the fluorescence such that the amplification was stopped during the exponential phase. Samples were removed from the plate and purified with SPRI beads using 70µl beads, no isopropanol, and eluting in 40µl of water. 1µl was used to measure the DNA concentration with a Qubit 3 and the provided reagents (Invitrogen, Cat#Q33218). 1 ng of DNA was used to check fragment size with a D1000 High Sensitivity Screentape and appropriate reagents (Agilent, Cat# 5067-5584, Cat# 5067-5585) on an Agilent 2200 Tapestation.

For MNase the libraries were sequenced (PE150) by Novogene Co. Ltd. ChIP-seq was sequenced by the BioMics facility of the Institut Pasteur.

6/ Cell-cycle RNA-seq.

Ccna-GFP *Sox2*-AID ES cells were cultured in the presence of 0.5mM of auxin (Sigma, Cat# I5148) for 3 hours. During the last 20 minutes 20µM Hoechst-33342 was added. Cells were trypsinised, filtered through a 40µm cell strainer and kept on ice. ES cells were sorted on the basis of Hoechst and GFP levels in three populations (early G1, late G1 and G2) using a FacsARIA III (Becton-Dickinson), keeping samples and collection tubes at 4 °C, as previously described (Festuccia et al. 2016). Data were analysed using the FlowJo software suite (Tree Star). Around 10^6 cells were sorted per population before RNA extraction with 1mL TRIzol (ThermoFisher, Cat# 15596026), according to the manufacturer's protocol. To eliminate any genomic DNA contamination, this was followed by an additional DNAse I treatment (Qiagen, Cat# 79254) for 20min at 37°C followed by phenol:chloroform purification. RNAs were resuspended in Ultrapure DNAse/RNase Free Distilled Water (Thermo, Cat# 10977035). Ribo-depleted, stranded and paired-end RNA-seq libraries were prepared and sequenced by Novogene Co Ltd.

7/ Western Blot.

For Western Blot analysis cell pellets corresponding to 10^6 cells were resuspended in 100 µl Laemmli Sample Buffer (BIO-RAD, Cat# 161-0737) containing β-mercaptoethanol. Lysed pellets were boiled for 10 min at 95°C and centrifuged for 10 min at maximum speed at room temperature.
Typically, 10 µl per sample was loaded on 4-15% Mini-PROTEAN TGX Stain-Free Gels (BIO-RAD, Cat# 4568086) and run in 1× SDS-Running Buffer (250 mM Tris/ 1.92 M Glycine/1% SDS) at 10-20 mA using the Mini-PROTEAN Tetra System (BIO-RAD). Proteins were transferred on a Protran nitrocellulose membrane (Amersham, Cat# 10600003) for 1 hour at 300mA using the wet transfer system (BIO-RAD) in 1× Transfer Buffer (10× 0.25M Tris/ 1.92M Glycine) prepared with a final concentration of 20% Ethanol. Membranes were blocked in PBST (PBS 0.1% Tween-20) 5% BSA for 1 hour at room temperature and incubated over night at 4°C with

primary antibodies (diluted in PBST 5% BSA). Excess antibodies were washed with PBST (5 washes, 5 min each) and incubated for 1 hour at room temperature in secondary antibodies HRP-conjugated (diluted in PBST 5% BSA). Membranes were washed 5 times, 10 min each at room temperature and incubated with PIERCE ECL2 Western Blotting Substrate (Thermo Scientific, Cat# 80196) 5 min in dark. After excess reagent was removed, proteins were visualised using the BIO-RAD Chemidoc MP Imaging System and processed using the Image Lab Software (BIO-RAD).
Antibodies used:
Primaries: anti-H3 (Abcam, Cat# ab1791) (1:5000), anti-SOX2 (R&D, Cat# AF2018) (1:500-1:1000)
Secondaries: anti-Rabbit IgG-HRP (Thermo Fisher, Cat# RB230254) (1:10.000), anti-Goat IgG-HRP (Thermo Fisher, Cat# 61-1620) (1:10.000)

8/ Computational Methods.

8a/ Data and availability.

Samples are summarised in Table S1. Briefly, at least 2 x Interphase and 2 x Mitosis ChIP-seq samples were sequenced for DSG+FA ESRRB, SOX2, POU5F1, NANOG; for SOX2 RNA-seq 3 x (EG1, LG1, G2) x (-Auxin, +Auxin) samples were sequenced. For nucleosome positioning and accessibility data , 3 x (0.5U, 16U, 128U) x (Interphase, Mitosis) for MNase-seq, 3 x (0.5U, 16U, 128U) x (Interphase, Mitosis) for MNase H3 ChIP and 2 x (Interphase, Mitosis) for ATAC-seq. Public datasets used in this study: Esrrb RNA-seq GSE75066 (Festuccia et al. 2016); ESRRB, SOX2, POU5F1 and NANOG FA ChIP-Seq GSE11431 (Chen et al. 2008); SOX2, POU5F1, NANOG FA ChIP-seq GSE11724 (Marson et al. 2008); SOX2, POU5F1, NANOG FA ChIP-seq GSE44288 (Whyte et al. 2013); SOX2 FA ChIP-seq GSE43275 (Aksoy et al. 2013); SOX2 Interphase and Mitosis FA ChIP-seq GSE89599 (Deluz et al. 2016); SOX2, POU5F1 Interphase Mitosis PFA ChIP-seq GSE92846 (Liu et al. 2017); POU5F1 G1, G2/M FA ChIP-seq GSE78073 (Shin et al. 2016).

8b/ TF binding in interphase and in mitosis.

Data Processing: reads were aligned with Bowtie 2 (Langmead and Salzberg 2012) to the mm9 genome, with options "-k 10". Reads were additionally filtered for those with a single discovered alignment (in Bowtie 2 "k" mode this is mapping quality = 255) and an edit distance less than 4. Determination of bookmarking requires a quantitative comparison of interphase and mitosis peaks. Reads mapping with identical coordinates may be genuine duplicate arising from distinct pull-down events, or artefactual PCR-duplicates. Care must be taken with the treatment of these duplicate reads, since the number of genuine duplicates is proportional to peak size (at very large peaks the number of genomic positions can become saturated). As peaks in mitosis are commonly smaller than in interphase, the inappropriate collapse of duplicate reads will degrade the quantitative signal in interphase over that in mitosis, and will therefore overestimate bookmarking signal. For libraries constructed with custom barcodes (Table S1), we can distinguish between genuine duplicates and PCR duplicates. For barcoded libraries the rate of genuine duplicate reads is 0.021 ± 0.012 (mean ± std., n=12) duplicates/read, with a maximum of 0.051 for a NANOG interphase replicate. In non-barcoded libraries total duplication (a mix of genuine and PCR duplicates) rate was 0.153 ± 0.225 (mean ± std., n=11). We found that these segregated into a high duplicate population with rates

above 0.1: 0.359 ± 0.282 (mean ± std., n=4) and a low duplicate population: 0.035 ± 0.017 (mean ± std., n=7, max. 0.060), whose duplication rate was in-line with the expected rate of genuine duplicates. We therefore collapsed duplicate reads in non-barcoded samples with a duplication rate > 0.1 (Supplemental Fig. 6; Table S1).

Peak calling: peaks were called against relevant inputs/controls for all samples using MACS2 (Feng et al. 2012) with "callpeak -q 0.2 -g mm". Peaks intersecting with the mm9 blacklist (ENCODE Project Consortium 2012) were excluded along with those on chrM and chrY. To determine a set of candidate binding we merged peaks in DSG+FA samples in interphase and mitosis. Peaks were further filtered to have (1) MACS2 FDR < 0.01 in both replicates in either interphase or mitosis, (2) a height > 0.8 reads per million (RPM) in at least one sample (a height of ~16 raw reads at our mean mapped read depth of ~20 million reads). The resulting peaks are a robust set of binding regions where there is sufficient quantitative information to asses bookmarking (Supplemental Fig. S6).

Bookmarking analysis: we take an approach similar to differential expression analysis in RNA-seq to determine the set of peaks bookmarked by ESRRB, POU5F1, SOX2 and NANOG. We combine the read counts for input and ChIP samples for a given TF in a single generalised linear model (GLM) aimed at assessing the difference between input and ChIP signal in both interphase and mitosis at each peak; we use the log link function:

$$\log \mu_{ij} = \sigma_j + \beta_{\mathrm{I}i} + \mathbf{1}_{\mathrm{TF}j}\beta_{\mathrm{TF}i} + \mathbf{1}_{\mathrm{M}j}\beta_{\mathrm{M}i}$$

Where μ_{ij} is the sample mean of peak i in sample j; σ_j is the library size factor for sample j; $\beta_{\mathrm{I}i}$ is the baseline log rate of reads in peak i; $\mathbf{1}_{\mathrm{TF}j}$ is an indicator variable determining whether the sample j corresponds to a ChIP or input sample; $\beta_{\mathrm{TF}i}$ is the log fold change in ChIP samples over input; $\mathbf{1}_{\mathrm{M}j}$ is an indicator variable determining whether the sample j is a mitotic sample; $\beta_{\mathrm{M}i}$ is the log fold change change in ChIP samples from interphase to mitosis. We assume that raw read count of each peak in each sample is negative binomially distributed according to $p_{ij} \sim \mathrm{NB}(\mu_{ij}, \alpha_i)$ for peak specific dispersion α_i. We implement this GLM using DESeq2 (Love et al. 2014). We expect the nearly all peaks will have significant differences between input and ChIP, and that the majority of peaks will have significantly different occupancy between interphase and mitosis. Therefore, we opted to not using the median geometric mean size factor estimation approach of DESeq2, and set the size factors to the total mapped reads of each sample. Within DESeq2 we encoded the indicator $\mathbf{1}_{\mathrm{TF}j}$ by a factor `ChipTF` and $\mathbf{1}_{\mathrm{TF}j}$ by a factor `ChipM`, and then we ran Wald tests on the model `~ChipTF + ChipM`. We tested `ChipTF` (the fold change of interphase over input), the sum `ChipTF + ChipM` (the fold change of mitosis over input), and finally `ChipM` the difference between interphase and mitosis. Each test was evaluated for significance with FDR < 0.05 and without the use of independent filtering. To determine the set of bookmarked peaks we required that a peak had differential occupancy (`ChipTF + ChipM`, FDR < 0.05), that both mitosis replicates had MACS2 FDR < 0.01 with one mitosis replicate had MACS2 FDR < 10^{-10}. Combined, this is a conservative strategy that helps ameliorate the effects of contamination from interphase cells. The significance of `ChipM` was further used to classify three types of bookmarking peaks with either higher enrichment in interphase (BI), in mitosis (BM), or similar in both phases (BS). This resulted in:

ESRRB: Lost (L): 23,787, BI: 2,848, BS: 5,762 and BM: 1,534 regions.
SOX2: L: 25,793, BI: 556, BS: 18 regions.
POU5F1: L: 16,293, BI: 76, BS: 25, BM: 1 regions.
NANOG: L 27,177, BI: 18 regions.

Visualisation and normalisation of ChIP-seq data: single end read data was extended to mean fragment length and plotted in units of reads per million for genome tracks and heatmaps; heatmaps are scaled to the median Interphase DSG+FA binding level and averaged to create meta plots. For scatter plots the number of reads intersecting with each peak was normalised by total mapped reads per library.

Gene Peak Proximity Enrichments: we determined whether genes responsive in EG1 to depletion of ESRRB or SOX2 were proximal to candidate ESRRB or SOX2 bookmark peaks (see RNA-seq analysis below). We calculated the distance between the TSS of each gene tested for differential expression to the set of candidate bookmark peaks. We then performed Fisher exact tests for the association between the set EG1 responsive genes to the set of all genes within xbp of a peak, for x in $[10^0, 10^8]$.

Transcription Factor Motif Detection: to discover transcription factor binding motifs in the mm9 genome assembly we used FIMO (Grant, Bailey, and Noble 2011) with parameters "--thresh 1e-3 --max-stored-scores 50000000" and supplied a 0-order Markov background file describing the relative nucleotide frequencies in the mm9 assembly. We scanned the mm9 genome for ESRRB motif MA0141.3 and POU5F1-SOX2 composite motif MA0142.1. We intersected these motifs with ESRRB, POU5F1, SOX2, and POU5F1-SOX2 peaks. Metaplots are centred on the best scoring motif within each peak.

8c/ Nucleosome positioning in interphase and in mitosis.

Data Processing: paired end reads were trimmed by aligning read pairs to discover regions of reverse complementarity surrounded by our custom adapters. Alignment and trimming were performed with the BioSequences package for Julia 0.6 (Bezanson et al. 2017). Reads were aligned to mm9 genome using Bowtie 2 (Langmead and Salzberg 2012) with options "-k 10 -I 0 -X 1000 --no-discordant --no-mixed", and filtered for reads with a single alignment mean edit distance less than 4 between read pairs. MNase-seq and MNase H3 ChIP-seq were sequenced with barcoded adapters, identical barcodes with identical position were collapsed.

Average Nucleosome profiles: to calculate the point clouds in Fig. 5 and Fig. 6 we scored the single base-pair corresponding to the mid-point of each fragment (140-200bp) to calculate the total number of mid-points relative to a feature of interest (TSS, EP300/ESRRB summits and ESRRB or POU5F1/SOX2 motifs). We normalised each mid-point by first a factor to account for enzymatic MNase cutting bias calculated for each read in each library, and second, by the sequencing depth of the library. To calculate the cutting bias we use a simplified version of the approach in (Martins et al. 2018), we evaluated the relative rates of occurrence of the k-mer at the end of each read and the total occurrence of that k-mer in the genome. Specifically, we took the two 6-mers lying over the end coordinates of each read, such that each 6-mer was composed of two 3-mers, one lying within the read and one lying outside. We counted total k-mers in the genome using the BioSequences package in Julia 0.6 (Bezanson et al. 2017). To assess an appropriate correction, we averaged the k-mers at the end of each read in a position weight matrix (PWM), we found the left PWM to be approximately equal to the reverse complement of the right PWM, and so we calculated a correction based on the left k-mer and the reverse complement of the right k-mer. If γ_i is the rate of occurrence of k-mer k_i

in the genome, ρ_i is the rate of occurrence of the same k-mer at MNase cutsites, and k_L is the left k-mer and $k_{R^\dagger}$ is the reverse complement of the right k-mer, then the correction factor for each read is given by:

To robustly evaluate nucleosome positioning signal we employed Gaussian process regression on the point clouds. We used a squared exponential covariance function and selected hyper-parameters for signal variance, length scale and noise variance, optimised on -500bp to +500bp window surrounding the central point of each analysed regions. For the most, this window contains the activity of interest and the covariances appear relatively stationary within this region as compared to outside where clearly the length and noise scales change as the data loses coherence. We selected hyperparameters by sparse gaussian process regression employing a variational approximation to the marginal likelihood (Titsias 2009) as offered by (https://github.com//SheffieldML//GPy), with an initial inducing input once per 10bp. We plot the Gaussian process mean. Finally, to assess nucleosome positioning signal between $\sqrt{\rho_L \rho_{R^\dagger} / \gamma_L \gamma_{R^\dagger}}$ interphase and mitosis we calculated the z-score (zero-meaned, standard deviation scaled signal) of the Gaussian process mean and scaled the data point clouds by the same values. This allows us to compare the relative positioning signal, rather than the absolute magnitude of nucleosome signal.

Differential nucleosome occupancy: To assess differential nucleosome occupancy between interphase and mitosis, we took the Gaussian process mean calculated from read-depth normalised, bias corrected MNase H3-ChIP read mid-points. We then calculated the ratio of mitosis over interphase of these Gaussian process means.

8d/ Chromatin accessibility in interphase and in mitosis.

Data Processing: paired end reads were trimmed by aligning read pairs to discover regions of reverse complementarity surrounded by Nextera sequencing adapters for ATAC-seq. Alignment and trimming was performed with the BioSequences package for Julia 0.6 (Bezanson et al. 2017). Reads were aligned to mm9 genome using Bowtie 2 (Langmead and Salzberg 2012) with options "-k 10 -I 0 -X 1000 --no-discordant --no-mixed", and filtered for reads with a single alignment mean edit distance less than 4 between read pairs.

Average accessibility profiles: the two end points (cut sites) of fragments in the 0-100 bp range, shifted inward by +/- 4bp as recommended (Buenrostro et al. 2013), where used to establish accessibility maps by counting their occurrence across the regions of interest centred on TSS, EP300/ESRRB summits and ESRRB or POU5F1/SOX2 motifs, normalised to the minimal value in +/-1kb window. This data was smoothed using Gaussian Process Regression, as described in the 'Average Nucleosome profiles' section.

8e/ RNA-seq Analysis.

Stranded paired end RNA-seq reads were aligned to the mm9 genome using STAR (Dobin et al. 2013) and quantified by RSEM (Li and Dewey 2011) using the RSEM-STAR pipeline, with additional options "--seed 1618 --calc-pme --calc-ci --estimate-rspd --forward-prob 0.0 --paired-end". RSEM estimated read counts per sample were rounded for use with DESeq2

(Love et al. 2014). Genes with at least 10 normalised counts in all replicates of at least one condition were considered for differential expression analysis. For all differential expression tests DESeq2 was run without independent filtering and without any fold change shrinkage, genes with padj < 0.05 are considered differentially expressed. Genes responding to ESRRB-depletion (GSE75066; Festuccia et al. 2016), or SOX2 Auxin-inducible degradation were determined at cell cycle stages early G1 (EG1), late G1 (LG1) and G2. We used a generalised linear model of negative binomially distributed read count data. We performed Wald tests under the model `~CC + TF + CC:TF`, where `CC` is a factor indicating cell cycle: EG1, LG1 or G2 and `TF` is a factor describing the presence or absence of the relevant `TF` in that sample. We tested the sum of `TF` and its interaction determine to determine a set of responsive genes in each stage of the cell cycle.

Supplementary references

Aksoy I, Jauch R, Chen J, Dyla M, Divakar U, Bogu GK, Teo R, Leng Ng CK, Herath W, Lili S et al. 2013. Oct4 switches partnering from Sox2 to Sox17 to reinterpret the enhancer code and specify endoderm. *EMBO J* **32**(7): 938-953.

Bezanson, J., A. Edelman, S. Karpinski, and V. Shah. 2017. "Julia: A Fresh Approach to Numerical Computing." *SIAM Review* 59 (1): 65–98.

Buenrostro JD, Giresi PG, Zaba LC, Chang HY, Greenleaf WJ. 2013. Transposition of native chromatin for fast and sensitive epigenomic profiling of open chromatin, DNA-binding proteins and nucleosome position. *Nat Methods* **10**(12): 1213-1218.

Chen X, Xu H, Yuan P, Fang F, Huss M, Vega VB, Wong E, Orlov YL, Zhang W, Jiang J et al. 2008. Integration of external signaling pathways with the core transcriptional network in embryonic stem cells. *Cell* **133**(6): 1106-1117.

Deluz C, Friman ET, Strebinger D, Benke A, Raccaud M, Callegari A, Leleu M, Manley S, Suter DM. 2016. A role for mitotic bookmarking of SOX2 in pluripotency and differentiation. *Genes Dev* **30**(22): 2538-2550.

Dobin A, Davis CA, Schlesinger F, Drenkow J, Zaleski C, Jha S, Batut P, Chaisson M, Gingeras TR. 2013. STAR: ultrafast universal RNA-seq aligner. *Bioinformatics* **29**(1): 15-21.

ENCODE Project Consortium. 2012. "An Integrated Encyclopedia of DNA Elements in the Human Genome." *Nature* **489** (7414): 57–74.

Feng J, Liu T, Qin B, Zhang Y, Liu XS. 2012. Identifying ChIP-seq enrichment using MACS. *Nat Protoc* **7**(9): 1728-1740.

Festuccia N, Dubois A, Vandormael-Pournin S, Gallego Tejeda E, Mouren A, Bessonnard S, Mueller F, Proux C, Cohen-Tannoudji M, Navarro P. 2016. Mitotic binding of Esrrb marks key regulatory regions of the pluripotency network. *Nat Cell Biol* **18**(11): 1139-1148.

Grant, Charles E., Timothy L. Bailey, and William Stafford Noble. 2011. "FIMO: Scanning for Occurrences of a given Motif." *Bioinformatics* 27 (7): 1017–18.

Langmead B, Salzberg SL. 2012. Fast gapped-read alignment with Bowtie 2. *Nat Methods* **9**(4): 357-359.

Li B, Dewey CN. 2011. RSEM: accurate transcript quantification from RNA-Seq data with or without a reference genome. *BMC Bioinformatics* **12**: 323.

Liu Y, Pelham-Webb B, Di Giammartino DC, Li J, Kim D, Kita K, Saiz N, Garg V, Doane A, Giannakakou P et al. 2017. Widespread Mitotic Bookmarking by Histone Marks and Transcription Factors in Pluripotent Stem Cells. *Cell Rep* **19**(7): 1283-1293.

Love MI, Huber W, Anders S. 2014. Moderated estimation of fold change and dispersion for RNA-seq data with DESeq2. *Genome Biol* **15**(12): 550.

Marson A, Levine SS, Cole MF, Frampton GM, Brambrink T, Johnstone S, Guenther MG, Johnston WK, Wernig M, Newman J et al. 2008. Connecting microRNA genes to the core transcriptional regulatory circuitry of embryonic stem cells. *Cell* **134**(3): 521-533.

Martins, André L., Ninad M. Walavalkar, Warren D. Anderson, Chongzhi Zang, and Michael J. Guertin. 2018. "Universal Correction of Enzymatic Sequence Bias Reveals Molecular Signatures of protein/DNA Interactions." *Nucleic Acids Research* 46 (2): e9.

Mueller F, Karpova TS, Mazza D, McNally JG. 2012. Monitoring dynamic binding of chromatin proteins in vivo by fluorescence recovery after photobleaching. *Methods Mol Biol* **833**: 153-176.

Shin J, Kim TW, Kim H, Kim HJ, Suh MY, Lee S, Lee HT, Kwak S, Lee SE, Lee JH et al. 2016. Aurkb/PP1-mediated resetting of Oct4 during the cell cycle determines the identity of embryonic stem cells. *Elife* **5**: e10877.

Titsias M. 2009. Variational Learning of Inducing Variables in Sparse Gaussian Processes. In *Proceedings of the Twelth International Conference on Artificial Intelligence and Statistics*, Vol 5 (ed. D David van, W Max), pp. 567--574. PMLR, Proceedings of Machine Learning Research.

Whyte WA, Orlando DA, Hnisz D, Abraham BJ, Lin CY, Kagey MH, Rahl PB, Lee TI, Young RA. 2013. Master transcription factors and mediator establish super-enhancers at key cell identity genes. *Cell* **153**(2): 307-319.